NEUROSCIENCE

Context-dependent regulation of Notch signaling in glial development and tumorigenesis

Rongliang Guo†, Danyu Han†, Xingrui Song†, Yanjing Gao, Zhenmeiyu Li, Xiaosu Li, Zhengang Yang, Zhejun Xu*

In the mammalian brain, Notch signaling maintains the cortical stem cell pool and regulates the glial cell fate choice and differentiation. However, the function of Notch in regulating glial development and its involvement in tumorigenesis have not been well understood. Here, we show that Notch inactivation by genetic deletion of *Rbpj* in stem cells decreases astrocytes but increases oligodendrocytes with altered internal states. Inhibiting Notch in glial progenitors does not affect cell generation but instead accelerates the growth of Notch-deprived oligodendrocyte progenitor cells (OPCs) and OPC-related glioma. We also identified a cross-talk between oligodendrocytes and astrocytes, with premyelinating oligodendrocytes secreting BMP4, which is repressed by Notch, to up-regulate GFAP expression in adjacent astrocytes. Moreover, Notch inactivation in stem cells causes a glioma subtype shift from astroglia-associated to OPC-correlated patterns and vice versa. Our study reveals Notch's context-dependent function, promoting astrocytes and astroglia-associated glioma in stem cells and repressing OPCs and related glioma in glial progenitors.

INTRODUCTION

The cerebral cortex consists of distinct neuronal and glial cell types assemble into functional circuits responsible for cognitive abilities. In the mammalian brain, radial glial (RG) cells are the major stem cells that directly give rise to neurons and glia or indirectly by generating intermediate progenitor cells during the cortical development (*1*, *2*). RGs in the cortex firstly differentiate into neurons at early stage and then switch to the glial fate that generates astrocytes and oligodendrocytes (*2*). Astrocytes, one of the principal subtypes of glial cells based on their star-shaped morphology, are required for modulating synaptogenesis and synaptic transmission, regulating water balance and ion homeostasis. They also participate in maintaining the blood-brain barrier integrity and immune response (*3*). Oligodendrocytes are another principal subtype of glial cells which form myelin to facilitate the transmission of electrical impulses. Beyond to myelination, oligodendrocytes are also involved in synaptic interaction, response to brain injury, and have great potential as glioma-initiating cells (*4*, *5*). These two cell types are tightly associated via secreted cytokines, chemokines, signaling molecules, and cell-cell contact during development and at the mature stage (*4*).

Multiple factors modulate gliogenesis, including Notch (*6*–*10*). Activation of Notch signaling requires cell-cell interaction, while ligands and receptors coexpress would result in cis-inhibition. Upon activation, the single transmembrane receptor encoded by Notch is cleaved and released the intracellular domain (NICD), which translocases to the nucleus and recruits the RBPJ as well as the cofactor like MAML1 (Mastermind-like) to modulate the target gene expression (*11*). Although Notch signaling in the glial development has been reported (*8*, *10*), the mechanisms of Notch in regulating cortical glial development at different stages and the correlated tumorigenesis are not understood well. The abnormal development of glia cells can disrupt central nervous system (CNS) homeostasis or result in severe neurological diseases, especially brain tumors.

In this study, we showed that deprivation of Notch signaling by deleting *Rbpj* in RG cells leads to an increase in oligodendrocyte production at the expense of astrocytes. Single-cell gene set variation analysis (GSVA) analysis showed that several metabolic pathways were changed due to the lack of Notch in these oligodendrocytes. Next, we investigated this phenotype in intermediate glial progenitor cells by deletion of *Rbpj* in *Olig2-Cre* mice. We found that neither the production of astrocytes nor oligodendrocytes is affected in the cortex. However, the developmental progress is accelerated in these Notch-deficient oligodendrocyte progenitor cells (OPCs), which is consistent with the finding that the growth speeds up in Notch-blocked OPC-correlated gliomas (*12*). In addition, cortical glial fibrillary acidic protein (GFAP) expression is up-regulated in astrocytes, although the general number of astrocytes remains unchanged in *Olig2-Cre*; $Rbpj^{F/F}$ mice. We identified a cross-talk between astrocytes and oligodendrocytes during the development by demonstrating that differentiating OPCs secrete Bone Morphogenetic Protein 4 (BMP4) to communicate with astrocytes that receive BMP4 to up-regulate GFAP expression, which might facilitate the synthesis and transport of lipids from astrocytes to oligodendrocytes to make myelin. *Bmp4* can be bound by RBPJ and regulated by Notch signaling. Last, similar to the generation switch from astrocytes toward oligodendrocytes, we revealed that deprivation of Notch signaling causes glioma subtype shift from an astroglia-associated toward an OPC-correlated pattern and vice versa.

RESULTS

Notch signaling promotes astrocyte generation in stem cells

RG cells give rise to both astrocytes and oligodendrocytes after completing neurogenesis in the cortex (*3*, *13*). To study the Notch

Key Laboratory of Birth Defects, Children's Hospital of Fudan University, State Key Laboratory of Medical Neurobiology and MOE Frontiers Center for Brain Science, Institutes of Brain Science, Fudan University, Shanghai, China.
*Corresponding author. Email: 14111520028@fudan.edu.cn
†These authors contributed equally to this work.

function in glial development, we first performed in utero electroporation (IUE) to eliminate cortical Notch signaling in the radial cells by knocking out *Rbpj* since the Notch receptor subtypes can compensate for each other (*14*, *15*) and all the four canonical activated Notch receptors must cooperate with RBPJ protein to regulate the transcription of downstream targets (*11*). The *pCAG-Cre* plasmids were electroporated into the cortex of *Rbpj* floxed mice at embryonic day 16.5 (E16.5; hereafter referred to as *pCAG-Cre; Rbpj*), a stage when cortical stem cells are transitioning from neurogenesis to gliosis (*16*), and the efficiency of *Rbpj* deletion has been validated (fig. S1A). H2B–green fluorescent protein (GFP) reporter mice in which the labeled GFP cells are located in the nuclei were used at P7. The SRY-box transcription factor (SOX10)–positive cells were considered as oligodendrocytes since it exclusively expresses in OPCs (*9*, *17*, *18*). SOX9 is a pan-astrocyte marker in the cortex despite that it also expresses in the early-stage OPCs (*19*, *20*). Therefore, the $SOX9^+/SOX10^-$ were considered as astrocyte lineage cells in the cortex. At postnatal day 7 (P7), we found that more than half of the GFP^+ cells were $SOX9^+/SOX10^-$ astrocytes, and the proportion of $GFP^+/SOX10^+$ oligodendrocytes was about 35% in the control mice (Fig. 1, A and B). However, the proportion of $SOX10^+$ cells was significantly increased to more than 95% in the *pCAG-Cre; Rbpj* conditional knockout cortex (Fig. 1, A and B). Besides, we also checked the expressions of Aldehyde Dehydrogenase 1 family member L1 (ALDH1L1) and Glutamine Synthase (GS), two pan-astrocyte markers (*21*, *22*), and these two proteins were almost colabeled, if not all, at P7 (Fig. 1A). We found that the proportion of $GFP^+/ALDH1L1^+/GS^+$ astrocytes was significantly decreased from more than 40% to less than 5% (Fig. 1B), indicating that the progeny of RG cell fate switches from astrocytes to oligodendrocytes after depriving Notch signaling.

Although the ratios of astrocyte-related markers, such as SOX9, ALDH1L1, and GS in H2B-GFP cells, were significantly reduced in *Rbpj* electroporated knockout cortex, we cannot rule out the possibility that Notch signaling is selectively required for these astrocytic genes, and oligodendrocyte markers are ectopically expressed in the absence of *Rbpj*. To further investigate this possibility, we bred *Rbpj* floxed mice with *IS* reporter mice in which cytoplasmic tdTOMATO would be expressed after CRE recombination (*16*) so that the morphology can be examined. Similar to the *Rbpj* and *H2B-GFP* floxed mice, the *pCAG-Cre* plasmids were electroporated into the cortex at E16.5 and analyzed at P21, a time point when glial development is largely completed. In the control mice ($Rbpj^{F/+}$; $IS^{F/+}$), both astrocytic and oligodendrocyte morphology cells spread out in the cortex and expressed SOX9 and SOX10, respectively (Fig. 1C). However, not only was the proportion of $SOX10^+$ cells significantly increased but most of the cells also resembled oligodendrocyte morphology (Fig. 1, C and D). Meanwhile, the ratio of $SOX9^+$ cells was markedly reduced to a very low level, and almost no canonical astrocytic morphology was found in the IUE area (Fig. 1, C and D). These data indicate that RG cells give rise to oligodendrocytes at the expense of astrocytes if Notch signaling is deprived.

To further explore the properties and roles of Notch signaling in cortical glial development, we performed single-cell RNA sequencing (scRNA-seq). We electroporated *pCAG-Cre* plasmids into the cortex of $Rbpj^{F/F}$; $H2B\text{-}GFP^{F/+}$ mouse embryos at E15.5 (Fig. 1E). At P1, we dissected and dissociated the IUE cortex, rostral migratory stream, and Olfactory Bulb (OB), followed by sorting and collecting the labeled GFP^+ cells using fluorescence-activated cell sorting. After this, scRNA-seq analysis was performed on the *pCAG-Cre;* $Rbpj^{F/F}$ sample (Fig. 1E). To better characterize the effect of Notch on glial cell development, we combined our previous scRNA-seq data as a control ($IS^{F/+}$, IUE at E15, sorted and analyzed at P1) (*16*). We removed endothelial cells, microglia, outlier cells, low-quality cells, doublets, and pyramidal neurons, as we focused on glial development. After quality control and filtering, a total of 12,491 cells (control: 4980 cells versus *pCAG-Cre;* $Rbpj^{F/F}$: 7511 cells) from the two samples were included and subjected to batch effect correction and cell cycle regression (fig. S1, C and D) (*23*).

Next, unsupervised clustering using Uniform Manifold Approximation and Projection (UMAP) generated a total of 18 clusters (fig. S1B). On the basis of canonical marker genes of distinct cell type, these clusters were divided into six major cell components (Fig. 1F and fig. S1, E and F) including OB_interneuron (e.g., markers *Dlx2*, *Sp8*, and *Dcx*), astrocyte (e.g., markers *Id3*, *Aldh1l1*, and *Aqp4*), RG cell (e.g., markers *Pax6*, *Gli3*, and *Gfap*), oligodendrocyte (e.g., markers *Pdgfra*, *Cspg4*, and *Sox10*), intermediate progenitor (e.g., markers *Olig2*, *Egfr*, and *Top2a*), and pyramidal neuron (e.g., markers *Eomes*, *Neurod6*, and *Pou3f1*) (Fig. 1, F and G). Please note that *Egfr* and *Olig2* are pan-glial marker at this stage as they are expressed in astrocyte, intermediate progenitor, and also oligodendrocyte (Fig. 1G and fig. S1E). In addition, we found that astrocyte and RG cell shared very similar expression profile, indicating that they are more closely related compared with other cell types (Fig. 1G). To further confirm that Notch signaling was blocked in *pCAG-Cre;* $Rbpj^{F/F}$ cells, we checked the expression of *Ascl1*, a canonical Notch signaling negatively regulated target (*24*–*26*) . Not only was the expression level of *Ascl1* increased but also the proportion of $Ascl1^+$ cells in *pCAG-Cre;* $Rbpj^{F/F}$ cells significantly increased (Fig. 1, H to J).

Next, we checked the ratios of glial-related cells between the two samples, we found that the ratios of radial glia and astrocyte decreased, but the ratios of intermediate progenitor and oligodendrocyte increased in *pCAG-Cre;* $Rbpj^{F/F}$ dataset (Fig. 1K), consistent with our previous results that disrupted Notch signaling in RG cells accelerates the differentiation of stem cells and promotes the generation of oligodendrocyte at the expense of astrocyte (Fig. 1, A to D).

We then performed GSVA analysis of oligodendrocytes between the two samples. The subcollection abbreviation was selected as the Kyoto Encyclopedia of Genes and Genomes (KEGG) pathway. We found that several pathways, like ribosome and DNA replication pathways, were increased in the absence of Notch. This indicated that although more oligodendrocytes are generated in Notch-deprived stem cells, the internal state of these oligodendrocytes was affected in the lack of Notch signaling, which may regulate the developmental process of oligodendrocytes (Fig. 1M). Similarly, we performed GSVA analysis of astrocytes, revealing that ribosome, DNA replication, and cell cycle pathways were also changed in astrocytes due to the lack of Notch signaling (Fig. 1M).

Because cortical stem cells also give rise to OB interneurons, the up-regulated proneural gene *Ascl1* expression after deleting *Rbpj* may facilitate OB interneuron production as well. To check this, we quantified the proportion of $DLX2^+/tdTOMATO^+$ cells in the electroporated subventricular zone (SVZ), showing that the ratio of $DLX2^+/tdTOMATO^+$ cells in $tdTOMATO^+$ cells was increased (Fig. 1L). This suggests that similar to the oligodendrocyte, OB

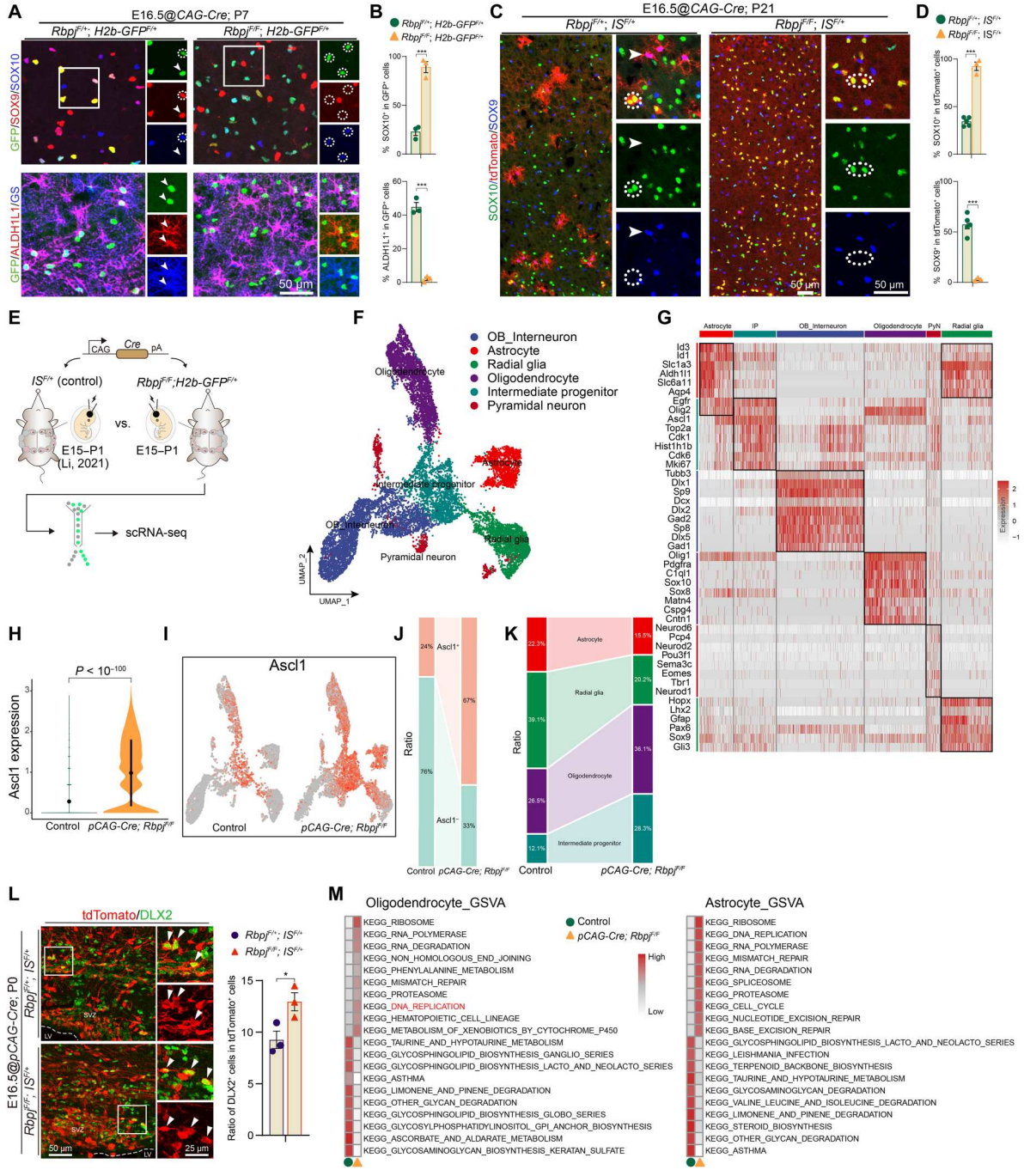

Fig. 1. Deprivation of Notch signaling in cortical stem cells results in generation of oligodendrocytes in the expense of astrocytes. (**A**) Representative immunostaining images of the P7 cortex stained for SOX9 and SOX10 with GFP (top), stained for ALDH1L1, and GS with GFP (bottom) of *Rbpj*$^{F/+}$*; H2B-GFP*$^{F/+}$ (control) and *Rbpj*$^{F/F}$*; H2B-GFP*$^{F/+}$ mice (IUE at E16.5). Dotted circles indicate oligodendrocytes. Arrowheads indicate astrocytes. (**B**) Quantification of the percentages of cortical SOX10$^+$ and ALDH1L1$^+$ cells in GFP reporter cells of *Rbpj*$^{F/+}$*; H2B-GFP*$^{F/+}$ and *Rbpj*$^{F/F}$*; H2B-GFP*$^{F/+}$ mice. (**C**) Representative immunostaining images of P21 cortex stained for SOX9 and SOX10 with tdTomato of *Rbpj*$^{F/+}$*; IS*$^{F/+}$ (control) and *Rbpj*$^{F/F}$*; IS*$^{F/+}$ mice (IUE at E16.5). Dotted circles indicate oligodendrocytes. Arrowheads indicate astrocytes. (**D**) Quantification of the percentages of cortical SOX10$^+$ and SOX9$^+$ cells in tdTomato reporter cells of *Rbpj*$^{F/+}$*; IS*$^{F/+}$ and *Rbpj*$^{F/F}$*; IS*$^{F/+}$ mice. (**E**) Schematic of the workflow of scRNA-seq analysis. (**F**) Uniform Manifold Approximation and Projection (UMAP) analysis of the integrated clusters after filtering the projection neurons. (**G**) Heatmap showing integrated cell cluster annotations ordered as UMAP. Columns represent individual cells; rows represent gene names. IP, Intermediate progenitor; PyN, Pyramidal neuron. (**H**) Feature plot of Ascl1 in control and *pCAG-Cre; Rbpj*$^{F/F}$ cells. (**I**) Violin plots showing increased *Ascl1* expression levels in *pCAG-Cre; Rbpj*$^{F/F}$ cells compared with control. (**J**) The proportions of *Ascl1*$^+$ and *Ascl1*$^-$ cells between the two groups. (**K**) The proportions of distinct clusters among the total cells in the distinct cluster. (**L**) Representative immunostaining images of P0 cortical SVZ stained for tdTOMATO and DLX2 of *Rbpj*$^{F/+}$*; IS*$^{F/+}$ (control) and *Rbpj*$^{F/F}$*; IS*$^{F/+}$ mice (IUE at E16.5). Dotted lines indicate the border of lateral ventricular (LV) and SVZ. Arrowheads indicate representative tdTOMATO$^+$/DLX2$^+$ cells. Right shows quantification of the ratio of DLX2$^+$ in tdTOMATO reporter cells. (**M**) GSVA analysis of oligodendrocyte and astrocyte clusters between control and *pCAG-Cre; Rbpj*$^{F/F}$ cells. A Student's *t* test was used for statistical analysis.

interneuron production is slightly increased after deletion of *Rbpj* in stem cells.

Deprivation of Notch signaling in intermediate glial progenitors does not result in cell fate and lineage commitment of astrocyte

The multipotent progenitor cells have the capacity, at least at population levels, to give rise to cortical astrocytes, oligodendrocytes, and OB interneurons (*16*). It remains unclear whether disruption of Notch signaling in these progenitor cells would reduce the astrocyte generation and increase the production of oligodendrocytes. To investigate this, we bred *Rbpj* floxed mice with the *Olig2-Cre* line that expresses CRE recombinase at progenitors but not stem cells in the cortex. We checked the efficiency of CRE recombinase and found significantly reduced RBPJ protein in *Olig2-Cre*; $Rbpj^{F/F}$ mice (fig. S2, A and B). At P0, we unexpectedly found that the numbers of SOX9, Oligodendrocyte transcription factor 2 (OLIG2), and Platelet Derived Growth Factor Receptor, alpha polypeptide (PDGFRA) were comparable between wild-type control and *Olig2-Cre*; $Rbpj^{F/F}$ conditional knockout cortices (Fig. 2, A and B). Because these genes are pan-glial markers at this stage (*22*), we checked the astrocyte-specific marker ALDH1L1 and found that the cell number did not show significant changes (Fig. 2, A and B). Besides, there was no significant difference in the number of $SOX10^+$ cells in cortex between wild-type and *Olig2-Cre*; $Rbpj^{F/F}$ mice (Fig. 2, A and B), suggesting that the generation of macro glia is relatively normal in progenitors without *Rbpj* and deprivation of Notch signaling in intermediate progenitor cells does not result in fate switching from astrocytes to oligodendrocytes.

Next, we double-checked this phenotype at P2, a stage that is just before the rapid amplification of cortical glia. We found no obvious differences in the numbers of $SOX9^+$, $OLIG2^+$, $PDGFRA^+$, and $AlDH1L1^+$ cells (fig. S2, C and D). Notably, the number of SOX10 cells in the cortex of *Olig2-Cre*; $Rbpj^{F/F}$ mice was slightly increased but showed no statistically significance (fig. S2, C and D).

We did not observe the astrocyte cell fate commitment in Notch-deprived progenitor cells, which might be because the fate determination of astrocyte in progenitor cells only has a very short time window and the already existing or not yet degraded RPBJ protein in *Olig2-Cre*; $Rbpj^{F/F}$ mice could help to go through that determination since the half-life of RBPJ can last for several hours to half a day, depending on cell type (*27*, *28*). Thus, to exclude this possibility, we developed an in vivo system to conditionally overexpress dominant negative *Maml1* (*dnMaml1*) (Fig. 2C), which inhibits the NICD-RBPJ complex immediately after it is translated (*29*). Because episomal plasmids in glial cells cannot be expressed, we constructed a Cre-dependent piggyBac (PB)–based reporter system to integrate into the genome, with the help of a nonintegrative *piggyBac transponsase* (PBase) plasmid (*30*), of the cortical stem cells through IUE (Fig. 2C). Target genes in the plasmids would be expressed in specific cell lineage under specific CRE recombination. We delivered the control plasmids (*PB-pCAG-floxed-STOP-floxed-GFP* (*PB-stop-GFP*) and *pCAG-PBase*) and *dnMaml1* conditional overexpression plasmids (*PB-pCAG-floxed-STOP-floxed-GFP-T2A-dnMaml1* (*PB-stop-dnMaml1*) and *pCAG-PBase)* to the cortex of *Olig2-Cre* embryos at E14.5 to E15.5. GFP^+ cells were almost all expressed in either $SOX9^+$ or $SOX10^+$ glial cells (Fig. 2D). We found that the ratios of $SOX10^+$ oligodendrocyte lineage and $SOX9^+/SOX10^-$ astrocyte lineage cells in total GFP^+ cells showed no remarkable alteration between control and *dnMaml1* cortex at E18.5 as well as P14 (Fig. 2, D and E, and fig. S2, E and F).

Although we did not find a significant change in either oligodendrocyte or astrocyte, we identified that the number of $SOX9^-/SOX10^+$ cells was increased in the cortex of *Olig2-Cre*; $Rbpj^{F/F}$ mice compared to the scarce $SOX9^-/SOX10^+$ cells in the cortex of wild-type control mice at P0 (Fig. 2, F and G). We suspected those increased $SOX9^-/SOX10^+$ precocious cells were due to the premature differentiation of Medial Ganglionic Eminence (MGE)–derived progenitors for two reasons. First, the prominent function of Notch signaling in stem cells is to maintain the progenitor pool which would be rapidly differentiated and exhausted in the absence of Notch signaling (*31*, *32*). Second, *Olig2* is also expressed in the MGE stem cells (*33*) that give rise to the first wave of cortical oligodendrocytes. Consistent with this idea, we crossed the *Rbpj* floxed mice with the *Nkx2.1-Cre* line that only labels the MGE-derived oligodendrocytes in the cortex. We found that the number of $SOX9^-/SOX10^+$ cells was increased in the cortex of *Nkx2.1-Cre*; $Rbpj^{F/F}$ mice (Fig. 2, H and I), indicating that the increased cortical $SOX9^-/SOX10^+$ cells in *Olig2-Cre*; $Rbpj^{F/F}$ mice is primarily due to the accelerated differentiation of MGE stem cells.

The growth of OPC is accelerated in the absence of Notch signaling

We did not observe a cell fate switch in the absence of *Rbpj* in multipotent progenitor cell lineage, but we found that the number of $SOX10^+$ cells was markedly increased in the cortex of *Olig2-Cre*; $Rbpj^{F/F}$ mice at P14 (Fig. 3, A and B). It is worth noting that we did not detect a significant difference in the number of $SOX9^+/SOX10^-$ astrocytes at this stage (Fig. 3, A and B). In addition, we chose S100beta (hereafter S100B), another astrocyte marker, to confirm this. Because S100B is expressed in both OPCs and astrocytes (*34*), the $S100B^+/SOX10^-$ cells were picked for quantifying. Consistently, we did not detect a significant difference in the number of $S100B^+/SOX10^-$ cells at P14 (Fig. 3B and fig. S3C), indicating that astrocyte number is still not affected at this stage. Besides, we also checked the apoptosis of glial cells using cleaved Caspase 3 with specific glial markers. We found that neither the total number of cortical apoptotic cells (total cleaved Caspase 3^+ cells) nor the number of apoptotic astrocytes (cleaved Caspase $3^+/ALDH1L1^+$ cells) at P5 was significantly changed in the *Olig2-Cre*; $Rbpj^{F/F}$ mice (fig. S3, D and E), indicating that the overall development of astrocytes is not affected.

We suspected that the increased number of $SOX10^+$ oligodendrocyte lineage cells could be due to an improved capacity for proliferation since we found that the DNA replication pathway is upregulated in the oligodendrocyte of *pCAG-Cre*; $Rbpj^{F/F}$ cells (Fig. 1M). Therefore, we next investigated the proliferation of glial cells by administrating 5-bromo-2′-deoxyuridine (BrdU; intraperitoneal injection) for 1 hour. We found that the number of $BrdU^+/SOX10^+$ oligodendrocytes, but not $BrdU^+/SOX9^+/SOX10^-$ astrocytes, was significantly increased at P2 in *Olig2-Cre*; $Rbpj^{F/F}$ cortices (Fig. 3, C and D). The increased $BrdU^+$ cells could still be detected at P14 or even later, although the absolute number of $BrdU^+$ cells was much lower compared with P2 (Fig. 3, C to F, and fig. S3A). Please note that almost all of these increased $BrdU^+$ cells at P14 coexpressed SOX10, indicating that they are OPCs (Fig. 3E). Moreover, in our scRNA-seq, we found not only the proportion of $Mki67^+$ cells

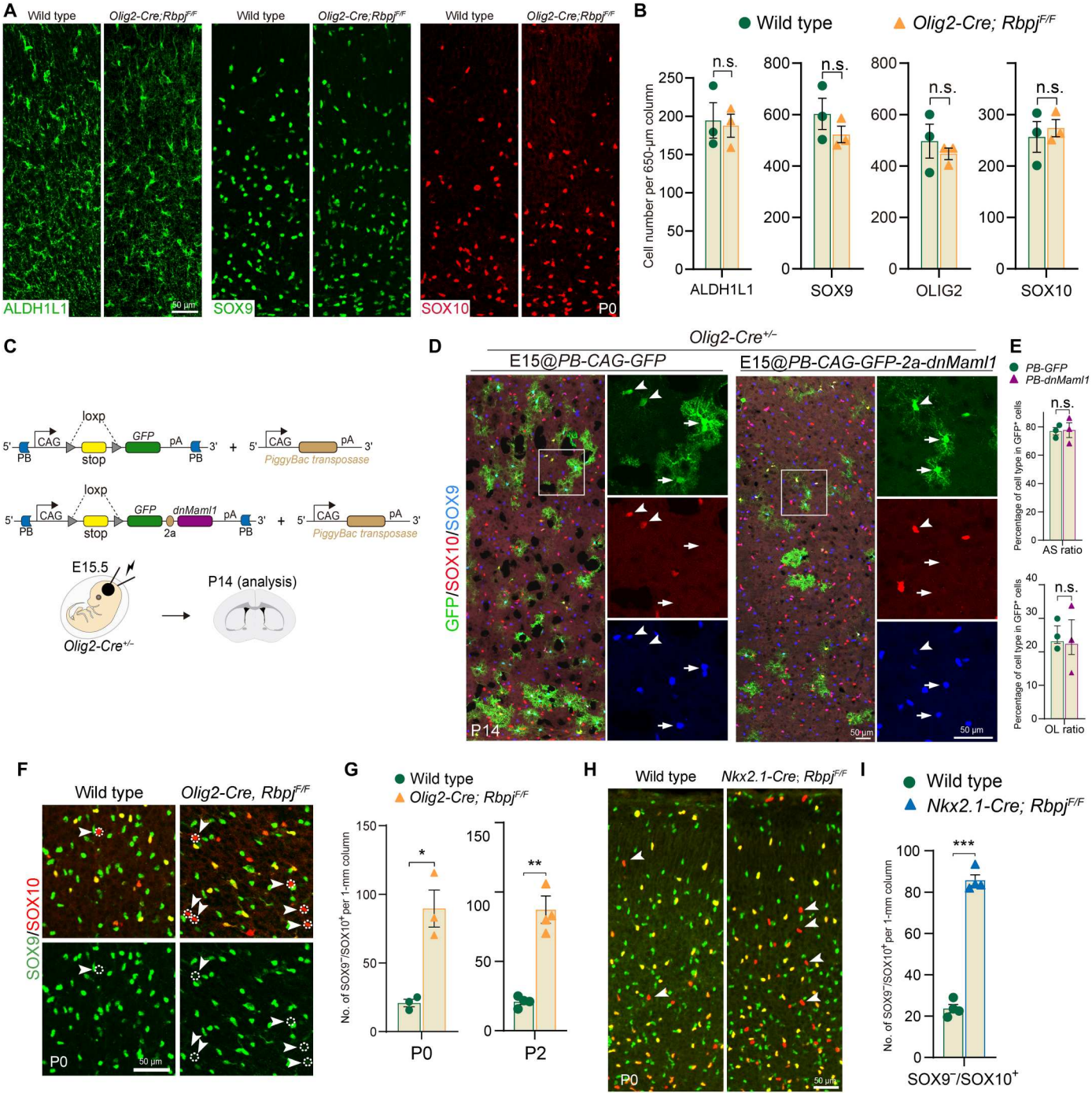

Fig. 2. Deprivation of Notch signaling in intermediate glial progenitor cells does not result in cell fate and lineage commitment of astrocyte. (**A**) Representative immunostaining images of P0 cortex stained for ALDH1L1, SOX9, and SOX10 in wild-type control and *Olig2-Cre; Rbpj*$^{F/F}$ mice. (**B**) Quantification of the cell numbers of ALDH1L1$^+$, SOX9$^+$, OLIG2$^+$, and SOX10$^+$ cells in the cortex of P0 wild-type control and *Olig2-Cre; Rbpj*$^{F/F}$ mice. (**C**) Schematic of the configuration and workflow of the control (*PB-stop-GFP*) and *PB-stop-dnMaml1* piggyBac transposon vectors. (**D**) Representative immunostaining images of P14 cortex stained for SOX9 and SOX10 with GFP of *Olig2-Cre*$^{+/-}$ mice IUE with control or *PB-dnMaml1* vectors at E15.5. Local magnification fields are shown in the relative right. Arrows indicate astrocytes (SOX10$^-$/SOX9$^+$). Arrowheads indicate oligodendrocytes (SOX10$^+$). (**E**) Quantification of the ratios of astrocytes and oligodendrocyte in GFP$^+$ reporter cells in the P14 cortex of *Olig2-Cre*$^{+/-}$ mice (IUE at E15.5). (**F**) Representative immunostaining images of P0 cortex stained for SOX9 and SOX10 in wild-type and *Olig2-Cre; Rbpj*$^{F/F}$ mice. Dotted circles with arrowheads indicate the SOX10$^+$/SOX9$^-$ cells. (**G**) Quantification of the numbers of SOX10$^+$/SOX9$^-$ cells in the wild-type and *Olig2-Cre; Rbpj*$^{F/F}$ mice at P0 and P2, respectively. (**H**) Representative immunostaining images of P0 cortex stained for SOX9 and SOX10 in control and *Nkx2.1-Cre; Rbpj*$^{F/F}$ mice. Arrowheads indicate the SOX10$^+$/SOX9$^-$ cells. (**I**) Quantification of the numbers of SOX10$^+$/SOX9$^-$ cells in the wild-type and *Nkx2.1-Cre; Rbpj*$^{F/F}$ mice at P0. A Student's *t* test (E, G, and I) or two-sided Mann-Whitney *U* test (B) was used for statistical analysis. n.s., not significant.

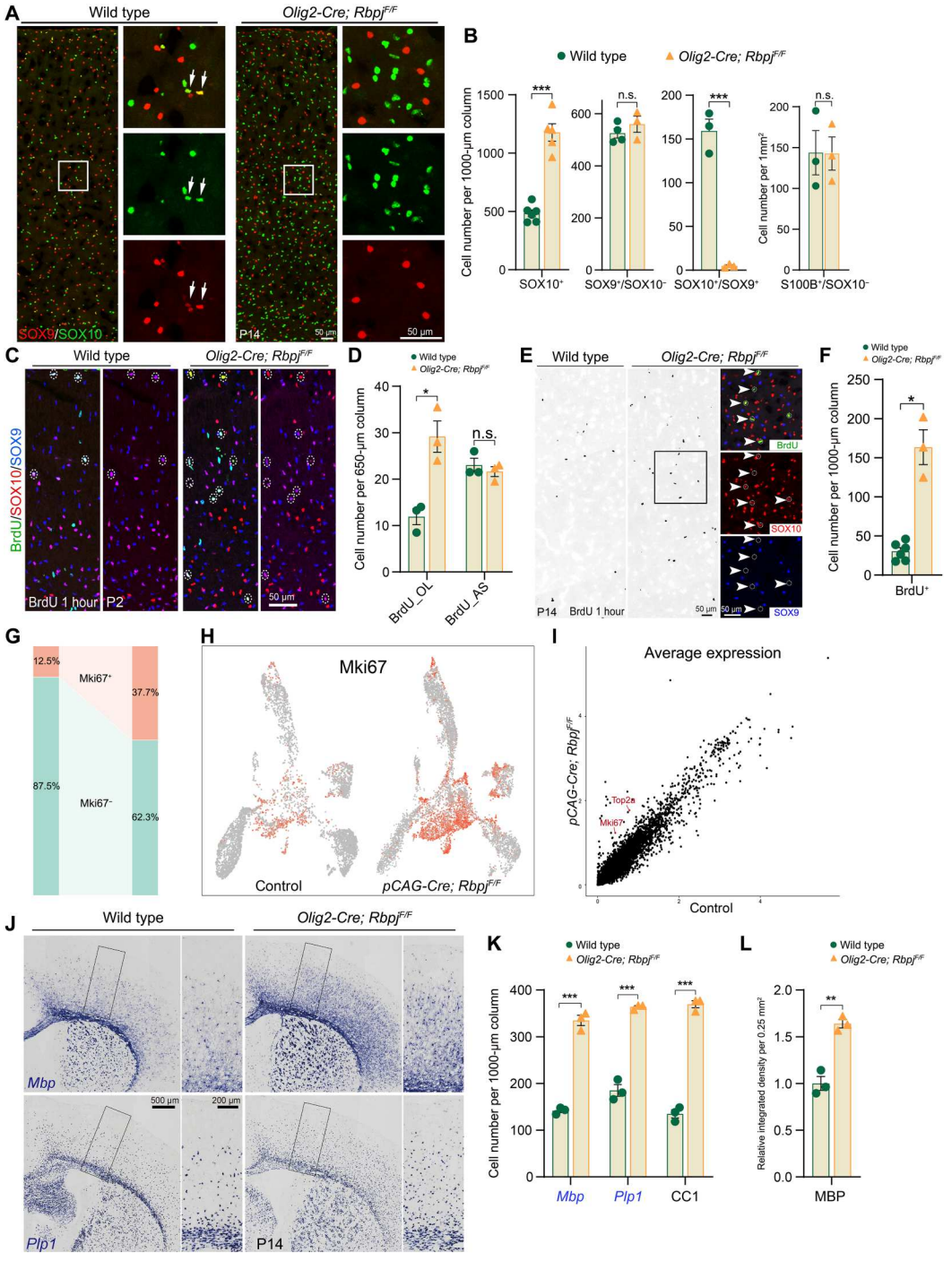

Fig. 3. Deprivation of Notch signaling in glial progenitor cells results in generating more oligodendrocytes due to increased proliferation. (**A**) Representative immunostaining images of P14 cortex stained for SOX9 and SOX10 in wild-type control and *Olig2-Cre; Rbpj*$^{F/F}$ mice. Arrows indicate coexpression. (**B**) Quantification of the cortical cell numbers of SOX10$^+$ (oligodendrocyte), SOX9$^+$/SOX10$^-$ (astrocyte), S100B$^+$/ SOX10$^-$ (mature astrocyte), and SOX9$^+$/SOX10$^+$ (immature oligodendrocyte) cells of P14 wild-type and *Olig2-Cre; Rbpj*$^{F/F}$ mice. (**C**) Representative images of P2 cortex stained for BrdU, SOX10, and SOX9 in wild-type and *Olig2-Cre; Rbpj*$^{F/F}$ mice. Dotted circles indicate BrdU$^+$/SOX10$^+$ coexpressed cells. BrdU_OL, BrdU$^+$/ SOX10$^+$; BrdU_AS, BrdU$^+$/SOX9$^+$/ SOX10$^-$. (**D**) Quantification of the cortical BrdU$^+$ cells of P0 wild-type and *Olig2-Cre; Rbpj*$^{F/F}$ mice. (**E**) Representative images of P14 cortex stained for BrdU in wild-type and *Olig2-Cre; Rbpj*$^{F/F}$ mice. Local magnification field shows the staining of BrdU, SOX9, and SOX10. Arrowheads with dotted circles indicate coexpression. (**F**) Quantification of the cortical cell numbers of BrdU$^+$ cells of P14 wild-type and *Olig2-Cre; Rbpj*$^{F/F}$ mice. (**G**) The proportions of *Mki67*$^+$ and *Mki67*$^-$ cells between the two groups. (**H**) Feature plot of *Mki67* in control and *pCAG-Cre; Rbpj*$^{F/F}$ scRNA-seq data. (**I**) Scatterplots show the expression levels of *Mki67* and *Top2a* in control and *pCAG-Cre; Rbpj*$^{F/F}$ cells. (**J**) Representative images of P14 cortex stained for *Mbp* and *Plp1* in wild-type and *Olig2-Cre; Rbpj*$^{F/F}$ mice. (**K**) Quantification of the cortical cell numbers of *Mbp*$^+$, *Plp1*$^+$, and CC1$^+$ cells of P14 wild-type control and *Olig2-Cre; Rbpj*$^{F/F}$ mice. (**L**) Quantification of relative integrated density of MBP protein in the P14 cortex of wild-type and *Olig2-Cre; Rbpj*$^{F/F}$ mice. A Student's *t* test (B, D, F, and L) or two-sided Mann-Whitney *U* test (K) was used for statistical analysis.

but also the expression level of *Mki67* as well as *Top2a* were increased in Notch-deprived OPCs (Fig. 3, G to I). In addition, Gene Ontology (GO) analysis of the up-regulated genes in progenitor cluster showed that most of the top 20 GO terms were related to mitosis in the absence of Notch (fig. S3B). Above all, these data suggest that the increased SOX10$^+$ cells in the *Olig2-Cre*; *Rbpj*$^{F/F}$ mice are caused by the improved proliferation of OPCs. This improved proliferation is consistent with previous study that deletion of *Rbpj* in glioblastoma, induced by *Pdgfb* overexpression and *P53* deletion, increases the proliferation and accelerates the growth of this tumor (*12*). We hypothesized that this might be correlated with the up-regulation of *Ascl1*, which is a specific target of Notch, which could bind to cell cycle–related genes and negatively correlated with glioma survival (*35*).

Next, we performed mRNA in situ hybridization of Myelin Basic Protein (*Mbp*) and Proteolipid Protein 1 (*Plp1*) and immunostaining of MBP and adenomatous polyposis coli (APC) clone CC1 (CC1) to assess whether those increased SOX10$^+$ cells could

differentiate into mature myelinated oligodendrocytes. We found that both the numbers of *Mbp*$^+$, *Plp1*$^+$, and CC1$^+$ cells and the density of MBP$^+$ myelin markedly increased in P14 *Olig2-Cre*; *Rbpj*$^{F/F}$ mice (Fig. 3, J to L, and fig. S3, F and G), indicating that not only did the number of the progenitor cells increase but also the population of mature oligodendrocytes expanded in the absence of Notch signaling in multipotent progenitor cells. In addition, we found that the fold changes of SOX10$^+$ and OLIG2$^+$ cells were relatively decreased at P30 compared with that at P14 (fig. S3, H and I). Together, these results indicate that loss of Notch signaling in progenitor cells accelerates cortical oligodendrocyte development. We hypothesized that the total number of cortical oligodendrocytes would tend to be comparable between *Olig2-Cre*; *Rbpj*$^{F/F}$ mice and the wild-type control at a very late stage. The reason may due to the largely unaffected generation of neurons in the cortex of the *Olig2-Cre* line, namely, the abundance of cortical neurons determines the number of oligodendrocytes ultimately.

GFAP expression is up-regulated in the cortex of *Olig2-Cre; Rbpj*$^{F/F}$ mice

Despite the total number of astrocytes showed no difference between wild-type control and *Olig2-Cre*; *Rbpj*$^{F/F}$ mice, we found that GFAP$^+$ cells were significantly increased in the cortex of *Olig2-Cre*; *Rbpj*$^{F/F}$ mice at P14 as well as P30 (fig. S4 and Fig. 4A), consistent with previous reports (*36*). We were interested in to what extent and in which part of the cortex GFAP increased in *Olig2-Cre*; *Rbpj*$^{F/F}$ mice. Regarding this, the cortical depth was divided into 10 bins of equal size at P30 (Fig. 4A). Normally, GFAP$^+$ cells are mainly located in the superficial layer (bin 1 and bin 2) and deep layer (bin 9 and bin 10), close to the meninge and corpus callosum, respectively. Scarce GFAP$^+$ cells can be found in the intermediate layer (bin 3 to bin 8) (Fig. 4, A and E). However, the total number of GFAP$^+$ cells was significantly increased, and the distribution of GFAP$^+$ cells became uniform in the cortex of *Olig2-Cre*; *Rbpj*$^{F/F}$ mice (Fig. 4A). The number of GFAP$^+$ in the superficial or deep layer showed no significant change, although bin 2 and bin 9 contained more GFAP$^+$ cells than controls (Fig. 4E). Nevertheless, GFAP$^+$ cells in the intermediate layer markedly increased in the cortex of *Olig2-Cre*; *Rbpj*$^{F/F}$ mice (Fig. 4D). Note that the cortical depth and the total number of SOX9$^+$ astrocytes were not altered (Fig. 4, B and C). In summary, these data indicate that the total number of astrocytes has not changed, but GFAP is up-regulated in the cortical astrocyte population in *Olig2-Cre*; *Rbpj*$^{F/F}$ mice.

Increased Bmp4 expression in oligodendrocytes induces the up-regulation of GFAP in the cortical astrocytes of *Olig2-Cre; Rbpj*$^{F/F}$ mice

To further assess the gene expression profile changes and the mechanism of cortical GFAP up-regulation in Notch-deprived progenitor cells, we performed bulk RNA-seq by sorting and collecting the cortical GFP$^+$ cells from *Olig2-Cre; H2b-GFP*$^{F/+}$ (control) and *Olig2-Cre; Rbpj*$^{F/F}$, *H2b-GFP*$^{F/+}$ mice at P2 (Fig. 5A). Differential gene expression analysis showed an increase in 522 mRNAs and a

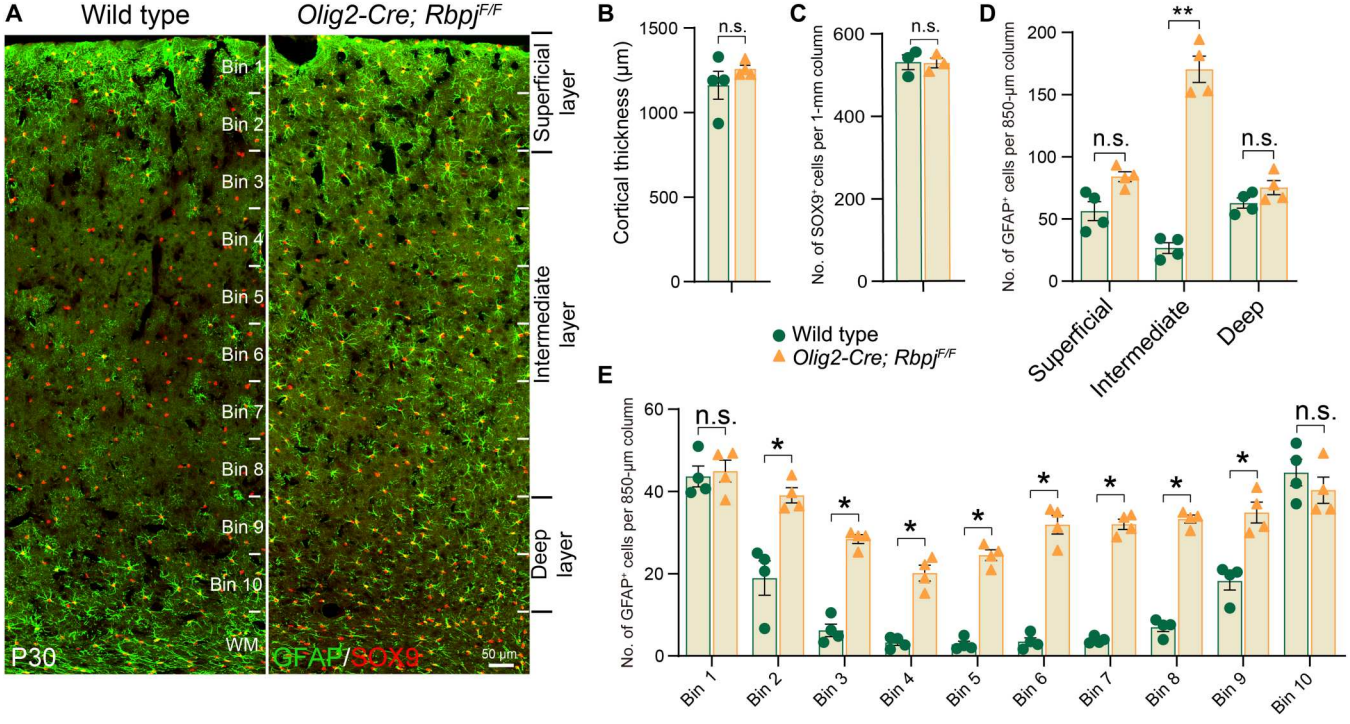

Fig. 4. GFAP expression is up-regulated in the cortex after depriving Notch signaling in the intermediate glial progenitor cells. (**A**) Representative images of P30 cortex stained for GFAP and SOX9 in wild-type and *Olig2-Cre; Rbpj*$^{F/F}$ mice. Cortex was equally divided into 10 bins. According to the normal expression of GFAP in the cortex, bin 1 and bin 2 define as superficial layer; bin 3 to bin 8 define as intermediate layer; bin 9 and bin 10 define as deep layer. WM, white matter. (**B** and **C**) Quantification of the cortical thickness (B) and the number of SOX9$^+$ cells (C) of P30 wild-type and *Olig2-Cre; Rbpj*$^{F/F}$ mice. (**D**) Quantification of the cell numbers of GFAP$^+$ cells in distinct layers of P30 wild-type and *Olig2-Cre; Rbpj*$^{F/F}$ mice. (**E**) Quantification of the cell numbers of GFAP$^+$ cells in each bin of P30 wild-type and *Olig2-Cre; Rbpj*$^{F/F}$ mice. A Student's *t* test (B, C, and E) or two-sided Mann-Whitney *U* test (D) was used for statistical analysis.

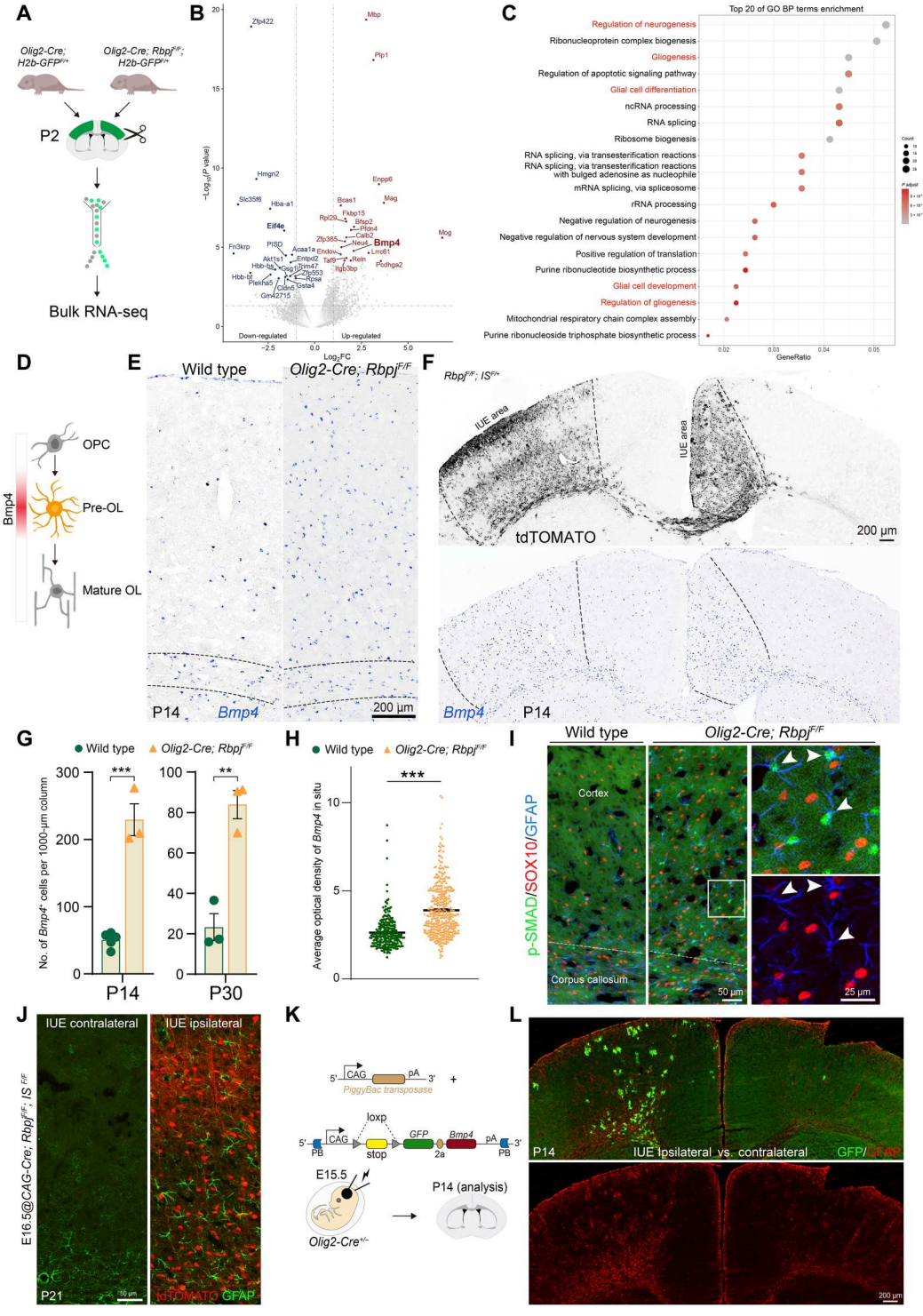

Fig. 5. Increased expression of Bmp4 in cortical oligodendrocytes responses for the non–cell autonomously up-regulated GFAP after depriving Notch signaling in progenitor cells. (**A**) Schematic of the workflow of bulk RNA-seq analysis. *Olig2-Cre; H2B-GFP*$^{F/+}$ (n = 3), *Olig2-Cre; Rbpj*$^{F/F}$*; H2B-GFP*$^{F/+}$ (n = 2). (**B**) Volcano plot showing the DEGs. Top 20 up-regulated and down-regulated genes in *P* value are highlighted. FC, fold change. (**C**) GO analysis of all the DEGs in our bulk RNA-seq. ncRNA, noncoding RNA; rRNA, ribosomal RNA. (**D**) Schematic of the expression pattern of *Bmp4* in oligodendrocyte development. (**E**) Representative images of P14 cortex stained for *Bmp4* mRNA in wild-type and *Olig2-Cre; Rbpj*$^{F/F}$ mice. Dashed lines indicate the border of white matter. (**F**) Representative images of P14 cortex stained for tdTOMATO or *Bmp4 (mRNA in situ)* in *Rbpj*$^{F/F}$*; IS*$^{F/+}$ mice which delivered *pCAG-Cre* plasmid at E15.5 by IUE. Dashed lines indicate the border of IUE and non-IUE area. (**G**) Quantification of the cell numbers of cortical *Bmp4*$^{+}$ cells in wild-type and *Olig2-Cre; Rbpj*$^{F/F}$ mice at P14 or P30. (**H**) Quantification of the average optical density of *Bmp4* mRNA in wild-type control and *Olig2-Cre; Rbpj*$^{F/F}$ mice at P14 (n = 3 for both groups, 239 cells from control, and 387 cells from experimental group). (**I**) Representative images of P14 cortex stained for p-SMAD1/5/9, SOX10, and GFAP in wild-type and *Olig2-Cre; Rbpj*$^{F/F}$ mice. Arrowheads indicate p-SMAD coexpresses with GFAP but not SOX10. (**J**) Representative images stained for GFAP and tdTOMATO in IUE contralateral and ipsilateral cortex of *Rbpj*$^{F/F}$*; ISJ*$^{F/+}$ mice at P21 (IUE at E16.5). (**K**) Schematic of the configuration and workflow of the *PB-stop-Bmp4* piggyBac transposon vectors. (**L**) Representative images of P14 cortex stained for GFP and GFAP in *Olig2-Cre* mice which conditionally overexpressed *Bmp4* after CRE recombination. A Student's *t* test was used for statistical analysis.

decrease in 244 mRNAs compared with the controls (table S1). The top 20 differentially expressed genes (DEGs) of both up-regulation and down-regulation in *P* values were shown in volcano plots (Fig. 5B). The top up-regulated genes were mainly oligodendrocyte related, like *Mbp*, *Plp1*, *Mag*, *Mog*, and *Bcas1*, consistent with our findings (Fig. 5B). The top down-regulated genes were *Zfp422*, *Hmgn2*, *Slc35l6*, *Eif4e*, and *Fn3krp* (Fig. 5B). GO analysis of all DEGs showed the top 20 biological process (BP) terms related to glial development, such as regulation of neurongenesis, gliogenesis, glial cell differentiation, and glial cell development (Fig. 5C). This reveals that disrupting Notch signaling in glial progenitor cells affects the cortical glial cell development.

Unexpectedly, we found that the expression of *Bmp4* was remarkably increased in the *Olig2-Cre; Rbpj*$^{F/F}$*, H2B-GFP*$^{F/+}$ mice

compared to wild-type controls (Fig. 5B and table S1). BMP signals have been reported to induce the astrocyte fate, especially up-regulate GFAP expression, and repress oligodendrocyte fate in a dose-dependent manner (*37*–*39*). Regarding this, we suspected that the increased expression of BMP4 might induce the up-regulation of cortical GFAP in the *Olig2-Cre; Rbpj*$^{F/F}$ mice. We then first confirmed the increase of *Bmp4* using RNA in situ hybridization at both P14 and P30 (Fig. 5, E and G). Note that although *Bmp4*$^{+}$ cells in the cortex were in a salt and pepper pattern in wild-type mice, relatively dense *Bmp4*$^{+}$ cells were located in the corpus callosum (Fig. 5E) where GFAP^{+} cells predominantly occupied normally. In addition, the *Bmp4* expression level in individual cells was also up-regulated in *Olig2-Cre; Rbpj*$^{F/F}$ mice at P14 by detecting the average optical density of mRNA in situ (Fig. 5H). Moreover, to determine which cell type expresses BMPs, we reanalyzed the scRNA-seq data of the adult frontal mouse cortex (*40*). *Aldh1l1* and *Sox9* expression revealed the astrocyte cluster (fig. S5A). The expressions of *Pdgfra*, *Olig2*, *Sox10*, *Plp11*, *Mag*, and *Mog* identified the distinct developmental stage of oligodendrocyte (fig. S5, B and C). We found that *Bmp4*, not *Bmp7*, is specifically expressed in premyelinating oligodendrocytes and, to a relatively lesser extent, in fibroblast cells and pericytes (Fig. 5D and fig. S5D). We also found that *Bmpr1b*, one of the BMP receptors, is predominantly expressed in astrocytes (fig. S5E). These data suggest that oligodendrocytes might communicate with astrocytes through BMP4 during myelination, and the mechanism of GFAP up-regulation in astrocytes is mainly a non–cell-autonomous manner. This means that increased cortical oligodendrocytes would secrete more BMP4 to promote GFAP expression in astrocytes.

Because knocking out Notch signaling in stem cells generates more oligodendrocytes, we checked whether *Bmp4* and GFAP expression were locally increased in the IUE area of *pCAG-Cre; Rbpj*$^{F/F}$*; IS*$^{F/+}$ mice. We found that the density of *Bmp4*$^{+}$ cells was significantly higher in the tdTOMATO^{+} region of *pCAG-Cre; Rbpj*$^{F/F}$*; IS*$^{F/+}$ mice (Fig. 5F). More GFAP^{+} cells were observed in *pCAG-Cre; Rbpj*$^{F/F}$*; IS*$^{F/+}$ ipsilateral cortex than either *pCAG-Cre; Rbpj*$^{F/F}$*; IS*$^{F/+}$ contralateral or *pCAG-Cre; Rbpj*$^{F/+}$*; IS*$^{F/+}$ control mice P21 (IUE at E15.5 to E16.5) (Fig. 5J), suggesting that cortical GFAP up-regulation is, at least in part, a non–cell-autonomous manner in *Olig2-Cre; Rbpj*$^{F/F}$ mice.

In addition, to investigate whether *Bmp4* is directly bound and repressed by Notch signaling, we inspected the binding sites of RBPJ and NOTCH in the cortex identified by Targeted DamID (*41*). We found that RBPJ can directly bind on the exon/intron (for different transcripts) of the *Bmp4* gene (fig. S5F). This indicates that *Bmp4* is directly repressed by Notch signaling during oligodendrocyte development.

Moreover, astrocytes produce lipids for oligodendrocytes to make myelin (*42*), and GFAP is required for the myelination of oligodendrocyte (*43*). Consistent with this, the GO analysis of the up-regulated DEGs in our bulk RNA-seq revealed that lipid metabolism–related terms were enriched (fig. S5G). We then checked the phosphorylated SMAD1/5/9 (p-SMAD1/5/9), the canonical targets of BMP signaling, expression in the brain. We only detected weak expression of p-SMAD1/5/9 in the corpus callosum of wild-type mice. p-SMAD1/5/9 expression in the wild-type cortex is almost at the background level (Fig. 5I). However, in *Olig2-Cre; Rbpj*$^{F/F}$ mice, we observed p-SMAD1/5/9^{+} cells in both the corpus callosum and cortex. Note that all these p-SMAD1/5/9^{+} cells did not express SOX10 but colabeled with GFAP (Fig. 5I) suggesting a paracrine function of Bmp signaling between oligodendrocytes and astrocytes. Last, to further confirm *Bmp4* function in oligodendrocytes, we designed to specifically express BMP4 in OPCs by delivering the *Bmp4* overexpression plasmid [*PB-pCAG-floxed-STOP-floxed-GFP-T2A-Bmp4* (*PB-stop-Bmp4*) and *pCAG-PBase*] to the cortex of *Olig2-Cre* embryos at E15.5 (Fig. 5K). We found that GFAP expression was up-regulated around the area where *Bmp4* is overexpressed (Fig. 5L). Together, these data suggest a cross-talk between oligodendrocytes and astrocytes at the premyelination stage. Namely, pre-oligodendrocytes secrete *Bmp4* to active GFAP expression in astrocytes, which may improve the synthesis or transport of lipids to support oligodendrocyte myelination (*42*, *43*).

Manipulation of Notch signaling in glioma stem cells affects the generation of glioma subtypes in vivo

Given that deprivation of Notch signaling in stem cells leads to the generation of astrocytes toward oligodendrocytes, we examined whether this mechanism applies to the formation of glioma subtypes since many developmental programs are reused during malignancy. In support of this, we developed an astrocytoma mouse model in vivo by delivering human *EGFRvIII* (*hEGFRvIII*) into the developing mouse cortex using the PB system (Fig. 6A). *EGFRvIII* is a tumor-specific mutation and a constitutively active form of epidermal growth factor receptor (EGFR) emerged by in-frame deletion of its two to seven exons (*44*). Overexpression of *EGFRvIII* in adult mouse brain fails to generate glioma (*45*), but delivering these vectors at P0 mice resulted in the development of neoplastic-like lesions by P14, which arose from the SVZ and spreading into the cortex and striatum (Fig. 6, B, D, and E). These lesions exhibited nodule-like structures and invaded perivascular regions with elongated and pleomorphic nuclei, all showing high levels of Proliferating Cell Nuclear Antigen (PCNA) and KI67 expression (fig. S6B), which are characteristic features of gliomas. Hematoxylin and eosin (H&E) staining showed that the pathology resembled astroglia hyperplasia (Fig. 6B). Furthermore, molecular analysis revealed that the majority of neoplastic cells were SOX9^{+}, with no detectable SOX10 expression at P14 (Fig. 6E). SOX10 was reported to be ubiquitously expressed in human gliomas but with varied levels (*46*). Oligodendroglioma, for instance, expressed high levels of SOX10, while astrocytoma exhibits relatively low intensity, which may be due to the presence of mixed oligoastrocytomas, as glioma stem cells have the potential to differentiate into both astrocytes and oligodendrocytes. Together, the pathology and molecular profile indicate that these lesions resemble astrocytoma.

Next, we combined *pCAG-Cre* and *hEGFRvIII* vectors in *Rbpj*$^{F/F}$ mice to assess whether depriving Notch signaling in these neoplastic cells would induce more oligodendrocyte lineages (Fig. 6, C and D). IUE at P0 analyzed at P14, we found that GFP^{+}/SOX10^{+} cells not only extensively distributed in the cortex but also located at the core of the nodules and/or were adjacent to the perivascular glioma cells (Fig. 6, E and F). The increased proportion of GFP^{+}/SOX10^{+} cells in Notch deprivation neoplastic cells (Fig. 6, E and F) was consistent with our previous observations. We double checked this phenotype in more malignant glioma in vivo induced by simultaneously overexpressing *hEGFRvIII* and dominant negative *P53* (*dnP53*) by IUE using the PB system (*PB-hEGFRvIII-dnP53*) (fig. S6D). The more serious tumor than that of a single *hEGFRvIII* induced was yielded after 2 weeks (at P14). These

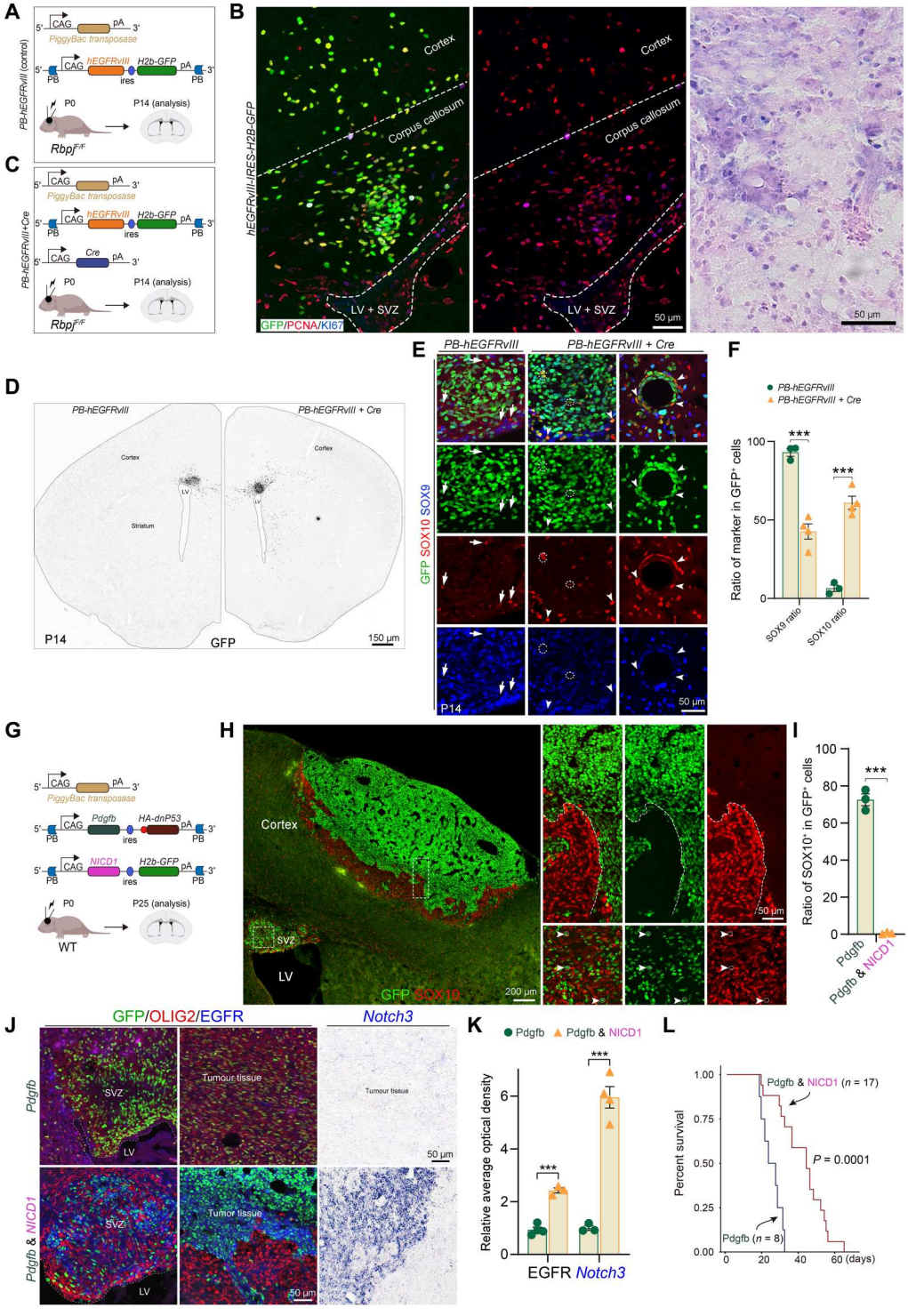

Fig. 6. Notch signaling regulates the generation of glioma subtypes in vivo. (**A**) Schematic of the configuration and workflow of the *PB-hEGFRvIII* piggyBac transposon vectors to induce neoplastic lesions. (**B**) Representative images of P14 sections stained for GFP, PCNA, and KI67 or H&E staining of mice delivered *PB-hEGFRvIII* vectors. (**C**) Schematic of the configuration and workflow of depriving Notch signaling in neoplastic lesion induced by *PB-hEGFRvIII*. (**D**) Representative images of P14 sections stained for GFP to show the general lesions induced by *PB-hEGFRvIII* with/without *pCAG-Cre*. (**E**) Representative images of P14 nodule-like structure and perivascular lesion stained for GFP, SOX10, and SOX9 in mice delivered *PB-hEGFRvIII* (control) or *PB-hEGFRvIII* and *pCAG-Cre* vectors. (**F**) Quantification of the ratios of SOX9$^+$ and SOX10$^+$ cells in GFP$^+$ cells in distinct lesions. (**G**) Schematic of the configuration and workflow of over activating Notch signaling in proneural subtype of glioblastoma. WT, wild type. (**H**) Representative images of P25 sections stained for GFP and SOX10 in proneural glioblastoma overexpressed Notch signaling. Dotted line indicates the expression border of GFP and SOX10. (**I**) Quantification of the ratio of SOX10$^+$ cells in GFP$^+$ cells in proneural glioblastoma (Pdgfb) or Pdgfb with NICD1. (**J**) Representative images of P25 sections stained for GFP, OLIG2, and EGFR or *Notch3* mRNA in situ in proneural glioblastoma (*Pdgfb-dnP53* as *Pdgfb*) or *Pdgfb* with NICD1 overexpression. (**K**) Quantification of the average optical density of EGFR in GFP$^+$ regions and *Notch3* in proneural glioblastoma (*Pdgfb*) or *Pdgfb* with *NICD1*. (**L**) Kaplan-Meier survival curves showing symptom-free survival of *Pdgfb-dnP53* (*Pdgfb*) versus *Pdgfb* and *NICD1* overexpression induced glioma mice. A Student's *t* test was used for statistical analysis.

neoplastic cells expressed a very low level of SOX10 in EGFR$^+$ cells. But SOX10 was expressed in those EGFR highly expressed regions (fig. S6E) when depriving Notch signaling, consistent with the above results.

We then investigated whether overexpression of active Notch in oligodendrocyte-correlated glioma cells would reverse it toward the astroglia-associated pattern. We delivered *Pdgfb* and *dnP53* overexpression vectors (Fig. 6G) to induce proneural GBM formation, an OPC-correlated GBM subtype (*PB-Pdgfb-dnP53*) (*47*, *48*). *PB-H2B-GFP* plasmids were delivered together with these tumor-induced vectors to label the mutant cells. In this glioma, the GFP$^+$/SOX10$^+$ malignant cells were ubiquitously spread and had a very high proportion (fig. S6F). To confirm this, we reanalyzed the previously published scRNA-seq data of retrovirus-expressing

Pdgfb-dnP53 for 35 days (*48*). Four major cell types were obtained in this proneural GBM subtype after filtering immune cells (fig. S6, A to C), consistent with our observation. Canonical OPC markers, like *Olig2*, *Pdgfra*, and *Sox10* (67.7%), were enriched in this GBM subtype (Fig. 6I and fig. S6, B and C).

We then overexpressed NICD1, the active form of the Notch1 receptor, in *PB-Pdgfb-dnP53*–induced GBM. We chose NICD1 because Notch1 is ubiquitously expressed in radial glia cells, progenitors, oligodendrocytes, and astrocytes (*16*). However, rarely $GFP^+/SOX10^+$ or $GFP^+/OLIG2^+$ cells were found after overexpressing NICD1 (Fig. 6, G to I). Actually, clear boundaries were observed between the GFP^+ cells and SOX10- and OLIG2-positive cells (Fig. 6, H to J). Moreover, we detected high expression levels of EGFR and *Notch3* in the NICD1 (GFP^+) overexpression region (Fig. 6, J and K). Please note that the expression of EGFR or *Notch3* in *Pdgfb-dnP53*–induced proneural GBM is very low (Fig. 6, J and K). In addition, more perivascular neoplasia was distributed in these NICD1 overexpression tumors (Fig. 6H), indicating that enhanced Notch signaling represses the expression of oligodendrocyte lineage genes in glioma. Previous report showed that deletion of *Olig2* causes reciprocal EGFR up-regulation and proneural to astrocytic phenotype shift of GBM (*47*). The lack of SOX10 and OLIG2 expression but reciprocal high levels of EGFR in NICD1 overexpression glioma cells are very similar to the phenotype of *Olig2* deletion. In addition, the enhanced EGFR and *Notch3* expression in glioma cells resembles the classical subtype of GBM (*49*). Together, these data reveal that the development of malignant glioma resembles the normal glial development procedures, and manipulation of Notch activity in glioma cells causes the glioma subtype shift.

To further investigate the effect of Notch signaling in glioma growth, we assessed the proliferation ability of OPC-correlated *Rbpj*-deleted glioma cells. The P0 cortex of $Rbpj^{F/F}$ mice was electroporated with *PB-Pdgfb-dnP53* [hemagglutinin (HA)–tagged] plasmid for 10 days followed by administering BrdU for 1 hour. The ratio of HA and BrdU double-positive ($HA^+/BrdU^+$) cells in total HA^+ glioma cells significantly increased after the deletion of *Rbpj* (fig. S6G). This indicates that, similar to OPC development (Fig. 7, A and B), the proliferation of OPC-correlated gliomas was precipitated by the loss of Notch signaling. In addition, the overexpression of NICD1 in *Pdgfb-dnP53*–induced gliomas extended the survival time of tumor-bearing mice (Fig. 6L). All of above, these data suggest that high Notch activity strongly correlates with distinct glioma subtypes and improves survival (Fig. 7), which is consistent with the previous study (*12*).

DISCUSSION

Notch signaling is required for glial development, but its function in distinct stages of glial development is not very clear. Here, we show that Notch-deprived stem cells generate fewer astrocytes but more oligodendrocytes with altered internal states or developmental processes (Fig. 7C). However, deprivation of Notch in intermediate glial progenitor cells does not result in generation changes of either astrocytes or oligodendrocytes but accelerates the developmental process of those Notch-deprived OPCs, as well as OPC-correlated gliomas. This is consistent with the previous results that OPC-correlated gliomas deteriorate rapidly after deleting *Rbpj* to inhibit Notch signaling (*12*). Moreover, we identified that BMP4, as a messenger, is secreted by oligodendrocytes to up-regulate GFAP expression in adjacent astrocytes (Fig. 7, A and B). Last, we in vivo investigated Notch signaling mediated glioma subtype shifts between astroglia associated and OPC correlated. In conclusion, we revealed a context-dependent function of Notch signaling that, when activated in stem cells, promotes the generation of astrocytes and astroglia-associated glioma. However, when activated in progenitors, it represses the growth of OPCs and related glioma (Fig. 7).

Blocking Notch signaling in OPCs leads to increased proliferation

The primary function of Notch signaling is to maintain the stem cell pool by promoting symmetric diversion and repressing the differentiation of stem cells. As a result, stem cells would rapidly undergo differentiation and expand the intermediate progenitors in the absence of Notch signaling. In this study, we found that the proliferation is increased in Notch-deprived OPCs. We speculate that this increased proliferation might consist of two stages. First, stem cells or early precursor cells accelerate differentiation at the neonatal period, in turn generating more progenitors due to the loss of Notch. We detected that increased cortical $BrdU^+$ cells in the *Olig2-Cre;* $Rbpj^{F/F}$ mice are owing to that most progenitors are mitotic cells. Second, those OPCs generated in the *Olig2-Cre;* $Rbpj^{F/F}$ mice would up-regulate *Ascl1* expression due to the lack of repression by Notch. *Ascl1* has been reported to control the production and promote the proliferation of OPCs (*50*, *51*). Moreover, *Ascl1* binds to the genes involved in cell cycle dependence, and deletion of *Ascl1* reduces the proliferation of OPC-related gliomas, reciprocally increasing the survival of tumor-bearing mice (*35*). Thus, the up-regulated expression of *Ascl1* could promote OPC proliferation in *Olig2-Cre;* $Rbpj^{F/F}$ mice. Please note that this high expression level of ASCL1 is not permanent but down-regulated during the maturation of OPCs for an unknown mechanism in these Notch-deprived OPCs, consistent with previous reports that *Ascl1* first up-regulates and then down-regulates in *Rbpj* deletion astrocytes (*24*, *52*). We believe that the relatively fewer $BrdU^+$ cells at P21 than at P14 in *Olig2-Cre;* $Rbpj^{F/F}$ mice are due to the down-regulation of *Ascl1*. In addition, a previous report showed that deletion of *Rbpj* accelerates OPC-related glioma growth, while genetically activating the Notch pathway in such gliomas reduces its growth and increases survival (*12*). This is consistent with our results, suggesting that Notch signaling represses OPC proliferation or growth.

Deprivation of Notch signaling in progenitor cells does not result in cell fate and lineage commitment of astrocytes

We identified a significant up-regulation of cortical GFAP in the *Olig2-Cre;* $Rbpj^{F/F}$ mice. A variety of conditions can lead to the up-regulation of GFAP, like reactive astrogliosis and glial scar formation in CNS lesions (*53*, *54*). Recently, a study showed that deletion of Pen-2, a subunit of γ-secretase, caused the up-regulation of GFAP due to the differentiation of OPCs into astrocyte fate by showing an increase in astrocyte gene expression, ALDH1L1 and GFAP, in both *Olig1-cre* and *NG2-CreER* lines (*36*). However, we did not identify an increase in the number of total astrocytes during development (P0 to P30). To quantify the number of astrocytes, $ALDH1L1^+$ and $SOX9^+/SOX10^-$ were applied at the neonatal period, while $SOX9^+$ and $S100B^+/SOX10^-$ were used at the postnatal stage in this study. Compared with ALDH1L1, SOX9 is also a pan-astrocyte marker, but it labels the nucleus making it easier to

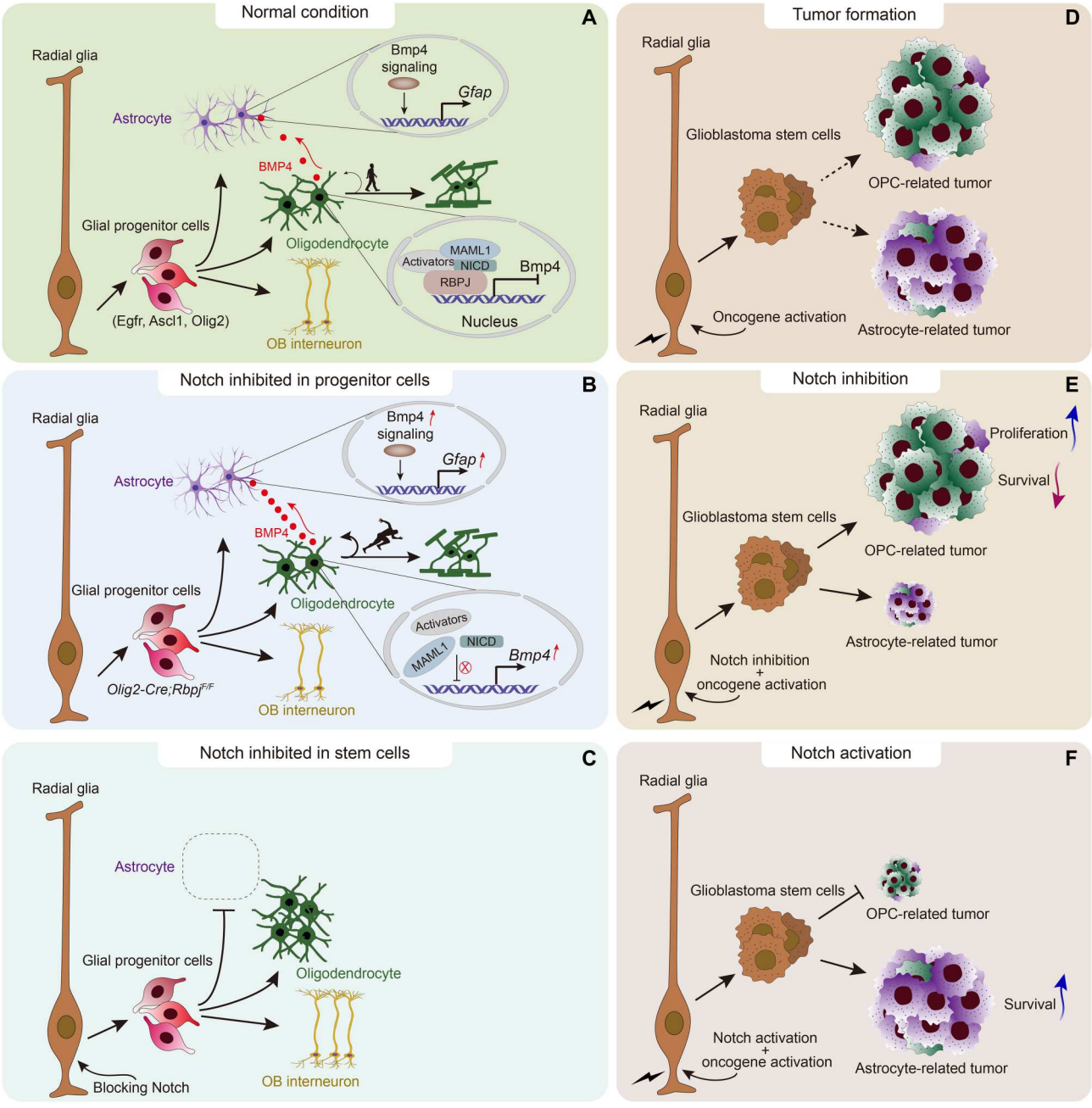

Fig. 7. Summary schema of Notch function in glial development and tumorigenesis (**A**) During later embryonic development, RG stem cells give rise to glial progenitor cells, which generate astrocytes, oligodendrocytes, and OB interneurons, respectively. Oligodendrocytes secrete BMP4 to astrocytes, which is repressed by Notch signaling, to induce GFAP expression during the maturation. (**B**) Inhibition of Notch signaling in intermediate glial progenitor cells does not affect the generation of astrocytes, oligodendrocytes, and OB interneurons. However, the lack of Notch accelerates the growth of oligodendrocytes, including proliferation and maturation. In addition, the expression of *Bmp4* is up-regulated and more secreted to astrocytes resulting in GFAP up-regulated in astrocytes. (**C**) Unlike the above regulation mode, blocking Notch signaling in RG cells inhibits the generation of astrocytes but reciprocally strongly promotes the generation of oligodendrocytes and slightly increases OB interneuron production. (**D**) RG cells have the potential to develop an OPC-related or an astrocyte-related glioma upon oncogene activation. (**E**) RG cells tend to generate an OPC-related glioma upon oncogene activation and simultaneous Notch inhibition. These OPC-related glioma cells without Notch signaling would increase the proliferation, similar to the OPC development in (B), and reduce the survival. (**F**) RG cells with strong Notch signaling tend to promote an astrocyte-related glioma and repress an OPC-related glioma upon oncogene activation. Besides, enhanced Notch signaling would improve the survival of tumor-bearing mice.

quantify than ALDH1L1 which would be influenced by the complex processes. After all, we did not observe an increase in the number of astrocytes. Moreover, fate mapping of *NG2-CreER* knock-in mice shows that lateral cortical, but not dorsal cortical, astrocytes can be labeled (*55*). *Rbpj* has been reported to affect the migration of cortical neurons (*56*); therefore, the possibility that the migration of OPCs is affected after deletion of *Pen-2* cannot be excluded. As a result, more ALDH1L1$^+$ and GFAP$^+$ cells might be included in the cortex due to migration changes. Considering that different genes are manipulated in our study and the *Pen-2* study, we cannot exclude the possibility that the differences in genes may have distinct functions, although they are involved in the same signal pathway.

Bmp4 mediates the cross-talk between oligodendrocytes and astrocytes

GFAP mutant mice show reduced thickness of the corpus callosum (*43*), indicating that it is required for myelination. Heterozygous mutation of *Gfap* in astrocytes results in Alexander disease, which exhibits abnormal aggregation and Rosenthal fibers (*57*). These fibers accumulate within the cytoplasm of astrocytes, inhibiting OPC proliferation and myelination (*58*), indicating a non–cell-autonomous regulation. In this study, we speculate that this GFAP up-regulation is, at least in part, a non–cell-autonomous manner through the increase of *Bmp4* secreted by the OPCs. Recently, a study of the Wnt effector *Tcf7l2* showed an autocrine function of *Bmp4* in repressing oligodendrocyte maturation in the spinal cord (*59*). They demonstrated that p-SMAD is colabeled with SOX10 in vitro. Similar to *Tcf7l2*, we found that *Bmp4* is repressed by Notch signaling as *Bmp4* expression is increased after deletion of *Rbpj* and RBPJ can directly bind to the *Bmp4* gene locus. However, detectable p-SMAD expression in vivo is restricted to astrocytes, especially GFAP$^+$ cells, in both control and these *Bmp4* up-regulated cells, suggesting a paracrine function of *Bmp4* in oligodendrocyte development and the communication between oligodendrocyte and astrocyte.

The communication between astrocytes and oligodendrocytes is critical for maintaining the integrity of the blood-brain barrier, immune response, and so on (*4*). Although studies have shown that astrocytes secrete platelet-derived growth factor, brain-derived neurotrophic factor, and other factors to promote oligodendrocyte proliferation and maturation (*60*–*62*), the cross-talk between oligodendrocytes and astrocytes is still not well understood. We speculate that OPCs secrete BMP4 to astrocytes at the beginning of myelination to inform astrocytes to synthesize or transport more lipids or other nutrients for myelin production. Up-regulation of GFAP could contribute to this synthesis or transport. According to the scRNA-seq, *Bmp4* is expressed in the meninges-related cells and immature oligodendrocytes, which are mainly located within the corpus callosum at the postnatal stage. This distribution of *Bmp4* is consistent with the expression of GFAP that is strongly expressed around the corpus callosum and meninges. Such a consistent expression pattern supports our hypothesis. Moreover, *Bmpr1b* is predominantly expressed in astrocytes, and p-SMAD is colabeled with GFAP. In addition, the GO analysis of up-regulated genes in our bulk RNA-seq shows enrichment of lipid metabolism. These data also support our hypothesis.

Moreover, a study of *Tcf7l2* showed an increase in *Bmp4* expression and a decrease in myelination (*59*). In this study, we observed both *Bmp4* and myelination to be increased at the postnatal stage, indicating that *Bmp4* does not inhibit myelination. Albeit *Bmp4* represses the generation of oligodendrocytes by promoting an astrocyte fate in vitro (*37*, *63*), Bmp signaling is required for the timely maturation of oligodendrocytes in vivo (*64*). We consider the oligodendrocyte inhibition function of Bmp to work in OPCs, the maturation-promoting function exerts in immature oligodendrocytes. Actually, BMP-induced astrocytes exhibit a cell cycle exited, typical mature pattern, indicating that Bmp signaling promotes the maturation of glia. Thus, we speculated that the increase of *Bmp4* in *Olig2-Cre; Rbpj*$^{F/F}$ mice not only serves as a messenger to communicate with astrocytes but also promotes cell cycle exit and maturation of OPCs.

Other mechanisms may also contribute to GFAP up-regulation when depriving Notch signaling in glial progenitor cells

Although deletion of *Rbpj* in adult astrocytes does not increase the expression of GFAP (*65*), we still cannot fully exclude a cell autonomous mechanism of GFAP up-regulation as we also found a decreased expression of *Eif4e* in our bulk RNA-seq. A study of *Eif4e* shows that reducing its phosphorylation would increase GFAP levels (*66*). The decrease of *Eif4e* expression may lead to a reduction of its phosphorylation level. In addition, GFAP up-regulation may also be correlated with the subtype change of astrocytes since cortical astrocytes contain multiple subtypes (*67*, *68*) and deprivation of Notch in developmental astrocytes may affect the generation of specific astrocyte subtypes. This speculation still needs further studies.

Notch signaling regulates the transformation of glioma subtypes

In this study, we found that the neoplastic lesion induced by *EGFR-vIII* resembles the astroglia-associated signature, which expresses SOX9 and GFAP but not SOX10. However, deprivation of Notch signaling leads to a significant increase in the ratio of SOX10$^+$ cells in the lesion, indicating a subtype shift of gliomas from astroglia-associated toward OPC-correlated. Apart from this knockout strategy, we overactivated NOTCH1 in OPC-correlated gliomas and reversely validated this phenotype. The gliomas with NICD overexpression showed almost undetectable SOX10 and OLIG2 expression. However, EGFR and *Notch3* are significantly up-regulated in these glioma cells. This is very similar to the previous study that showed deletion of *Olig2* in proneural subtype leads to increased expression of a set of classical signature genes, especially EGFR, thus leading to a subtype switch (*47*). Gliomas contain stem-like cells that are highly tumorigenic but phenotypically reminiscent of neural stem cells (*69*, *70*). Although which cell type initiates gliomas remains controversial (*5*, *71*), neural stem cells can be an important origin since both oligodendrocytes and astrocytes are derived from them. In this study, we demonstrated that enhancing Notch signaling in gliomas would induce the generation of astroglia-associated tumors. However, deprivation of Notch in stem cells would result in glioma subtype shifts toward OPC-correlated and, in progenitor cells, would increase proliferation, thus accelerating the growth of OPC-correlated gliomas. Considering that a brain tumor often contains heterogeneous cell types, enhancing Notch signaling conjunction with medicine that specifically target astroglia-associated gliomas may achieve a better effect.

MATERIALS AND METHODS

Mice

All mouse experimental procedures were performed in compliance with the National Institutes of Health Guide for the Care and Use of Laboratory Animals and were approved by the Animal Ethics Committee of Fudan University. We used *hGFAP-Cre* (*72*), *Rbpj floxed* (*73*), *Olig2-Cre* (*74*), *Nkx2.1-Cre* (*75*), and either *Rosa-H2B-GFP floxed* (*76*) or *Rosa-IS floxed* (*76*) for genetic fate mapping. *Wild-type* or littermates without the *Cre* allele were considered as controls. Littermates were assigned without discrimination of sexes to each experimental condition. Transgenic mice used in this study were on a compound background of C57BL/6j, 129S6, and ICR (CD1).

Mice were allowed ad libitum to water and food and maintained on a 12-hour light/dark cycle. The plug date was considered E0.5, and the day of birth was defined as P0.

Mouse tissue preparation

For fixed tissues, anesthetized mice were briefly perfused with ice-cold phosphate-buffered saline followed by 4% paraformaldehyde thoroughly. Brains were collected and postfixed in 4% paraformaldehyde overnight at 4°C. After dehydration in 30% sucrose, brains were embedded in optimal cutting temperature and preserved at −80°C. All mouse frozen tissues were sectioned into 20-μm thickness, unless specifically mentioned, and stained on glass slides. Fresh tissues were collected for scRNA-seq or bulk RNA-seq. Tissues were rapidly isolated without perfusion from deeply anesthetized mice and dissociated into single cells for cell sorting to perform either scRNA-seq or bulk RNA-seq.

Plasmid construction

pCAG-Cre vector was reported elsewhere (*16*). To construct the *pCAG*-PBase vector, the coding sequence (CDS) of *Cre* in the *pCAG-Cre* vector was replaced by the PBase. To construct the PB-pCAG-H2B-GFP vector, the CDS of *Cre* in the *pCAG-Cre* vector was replaced in-frame with *H2b-gfp* from the Rosa-H2B-GFP mice. The inverted terminal repeat sequence of the PB transposon was cloned into the upstream of the CAG promoter and downstream of the b-globin polyadenylation (polyA) sequence for recognition by the PBase

For direct overexpression vectors, like overexpression of *hEGFR-vIII*, NICD1, the targeted CDS was cloned into the downstream of the CAG promoter. Internal ribosomal entry site sequence was placed between the targeted CDS and the GFP reporter. For tumor-inducing vectors, *hEGFRvIII* or *Pdgfb* was cloned into the downstream of the CAG promoter, and *Gfp* was replaced by an HA-tagged dnP53. For conditionally overexpression vectors, like *STOP-dnMaml1* and *STOP-Bmp4*, 3× SV40 polyA sequence and 1× bGH polyA sequence flanked by Loxp were used to prevent transcription without *Cre* recombination. This Loxp-STOP-Loxp cassette and the targeted CDS plus GFP reporter were cloned into the downstream of the CAG promoter using the In-Fusion cloning kit (Novoprotein).

In situ hybridization

In situ hybridization was performed as previously described using digoxigenin-labeled riboprobes (*77*). Riboprobes were amplified by polymerase chain reaction using the following primers (5′-3′): *Bmp4-F*: ACCGAATGCTGATGGTCGTT; *Bmp4-R*: AATGGCGACGGCAGTTCTTA; *Plp1-F*: AGGACAGAAGAAGGAGACTGGAGAGAC; *Plp1-R*: GTGGTCTTGTAGTCGCCAAAGATCTGC; *Mbp-F*: GAAGAGACAGCCGCTCTGGATCTC; *Mbp-R*: ATGGTGACATTTGGCGGCCAC; *Notch3-F*: GATGCCAGCAGGATGTGGAT; *Notch3-R*: CGTACGGGTAGTCACTGTGAACAC.

Immunofluorescence staining and histology

Immunohistochemistry was performed as previously described (*78*). Briefly, slices were washed three times with tris-buffered saline (TBS) and incubated in primary donkey serum blocking buffer (5% donkey serum and 0.5% Triton X-100 in TBS) at room temperature (RT) for 1 to 2 hours. Primary antibodies diluted in blocking buffer were incubated overnight at 4°C. Slices then were transferred to the RT and washed three times. Alexa Flour–labeled secondary antibodies were resuspended in half concentration of primary donkey serum blocking buffer (diluted with TBS) and incubated with slices for 2 hours at RT. Slices were mounted after washing twice. 4′,6-Diamidino-2-phenylindole was used to visualize nuclei. For BrdU staining, slices were soaked in 2 N HCl for 1 hour followed by rinsing in 0.1 M borate buffer twice at RT before the regular immunohistochemistry procedure.

Immunofluorescence staining was performed with the following primary antibodies: rabbit anti- ALDH1L1 (Abcam, ab10712968), rat anti-BrdU (Accurate Chemical, OBT0030s), goat anti-EGFR (R&D Systems, AB-355937), rabbit anti-GFAP (Dako, Z0334), rabbit anti-GFP (Aves Labs, GFP-1020), rabbit anti-Glutamine synthetase (Oasis Biofarm, N2110151), rabbit anti-KI67 (Abcam, ab15580), rabbit anti-OLIG2 (Millipore, AB9610), mouse anti-OLIG2 (Millipore, MABN50), mouse anti-PCNA (Abcam, ab29), rat anti-PDGFRA (BD Pharmingen, 558774), rabbit anti-pSMAD1/5/9 (Cell Signaling, 13820), rabbit anti-RBPJ (Cell Signaling, 5313T), rabbit anti-S100B (Dako, Z0311), goat anti- SOX10 (R&D Systems, AB-442208), guinea pig anti-SOX10 (R&D Systems, AF2864), rabbit anti-SOX9 (Abcam, ab185966), goat anti-tdTOMATO (OriGene, AB8181), rat anti-CC1 (Oasis Biofarm, OB-PRT039), rabbit anti–cleaved Caspase 3 (Cell Signaling, 9915), and rat anti-MBP (Millipore, MAB386).

H&E staining was performed on 20-μm cryostat sections to analyze the tumor pathology. The classification of tumor subtype was assigned using the World Health Organization grading.

Image acquisition and analysis

Stained tissue sections were imaged on an Olympus BX 51 microscope or an Olympus FV3000 confocal microscope system. Tiled fields were stitched using a 15% overlap. Images were processed by Adobe Photoshop CC software.

ImageJ software was applied to evaluate the expression level, determined by average optical density (EGFR, *Bmp4*, and *Notch3*) and the overall population of myelin, defined by integrated density (MBP).

BrdU administration

Intraperitoneal injection was used for BrdU administration (50 mg/kg body weight). Tissues were isolated and analyzed 1 hour after administration.

In utero electroporation

The IUE procedure was performed according to a previous study (*16*) using a BTX830 electroporator and 7-mm platinum electrodes. Briefly, timed-pregnant mice were anesthetized with isoflurane (4% isoflurane for induction, 2% isoflurane for maintenance). Plasmid solutions containing DNA (1.5 to 2 mg/ml) and 0.05% Fast Green were administered into the lateral ventricle of embryos (0.5 μl each) using a beveled capillary. Five pulses (lasting 50 ms each) with an interval of 950 ms were applied. The voltages were optimized as 35 V for E15 and E16 and 29 V for E14.

Bulk transcriptome sequencing

Cortices were dissected from *Olig2-Cre, Rbpj*$^{F/F}$, *H2B-GFP* $^{F/+}$ mice ($n = 2$) and littermate controls (*Olig2-Cre, Rbpj* $^{F/+}$, *H2B-GFP* $^{F/+}$; $n = 3$) at P2. Tissues were dissociated into single cells, and fluorescent cells, approximately 0.35 to 0.45 million cells from two embryos, were sorted and collected by flow cytometry. After RNA extraction and quality control, cDNAs were generated and amplified using the SMART-Seq HT kit (catalog no. 634437, Takara) according to the manufacturer's protocol. RNA-seq libraries were prepared by the Ovation Ultralow Library System V2 kit (Nugen, 0347), quantified by Qubit 2.0 Fluorometer (Invitrogen), checked with Agilent 2100, and loaded onto the Illumina HiSeq 2500 for sequencing. Gene expression levels were reported in fragments per kilobase of exon model per million mapped fragments (FPKM). DEGs were defined as $P < 0.05$.

Single-cell RNA sequencing

scRNA-seq library preparation was described elsewhere (*16*). Briefly, *pCAG-Cre* vectors were delivered into the cortex of *Rbpj*$^{F/F}$; *H2B-GFP*$^{F/+}$ embryos at E15.5. These cortices were dissected and dissociated into a single-cell suspension at P1 followed by fluorescence-activated cell sorting to collect GFP$^+$ cells. The scRNA-seq libraries were generated by the Chromium droplet-based sequencing platform (10X Genomics) according to the manufacturer's instructions (manual document part number: CG00052 Rev C). After purification and quantification, the cDNA libraries were sequenced on an Illumina HiSeq4000.

After removing low-quality sequences and adapters, high-quality sequences (clean reads) were obtained. Cell Ranger software was used to process these clean reads to obtain quantitative information on gene expression. Cells with fewer than 200 detected genes or a mitochondrial gene ratio of more than 10% in controls or more than 5% in the experimental group, as well as genes expressed in fewer than three cells, were filtered out. The sctransform package was used to perform normalization and variance stabilization of the two datasets. The datasets were batch-corrected using Harmony V1.0 and clustered using Seurat V4.0.0. Cell cycle regression was performed, and the difference between G_2M and S phase scores was regressed out. Seurat V4.0.0 was used to identify specific marker genes of clusters and visualization with dot and feature plots. The R package of GSVA was used to perform single-cell GSVA analysis, and the top sigRnificant pathways were shown.

Functional analysis by enrichment analysis

GO analysis was applied to the statistically significant expression genes to verify its biological functions and pathways using R software. *P* values were adjusted by false discovery rate for significant enrichment, and the top 20 enrichments were shown.

Single-cell GSVA was implemented in R software using the GSVA package. MSigDB subcollection abbreviation was selected as the KEGG pathway. The calculation of enrichment score for each sample and pathway was based on a nonparametric unsupervised approach. Each of the top 15 enrichment pathways in each sample was shown.

Quantification and statistical analysis

For individual experiments, at least three samples of control or mutant mice were examined. Multiple sections from individual brains at similar positions were analyzed in morphological experiments. The analyzed mice were littermates of both sexes and age-matched. Investigators were not blinded to mouse genotypes during analysis. Values and error bars represent the mean ± SEM. The respective replicate number (n) is indicated in the figures. Statistical comparisons were performed using R. *P* values were determined by an appropriate statistical test, such as a Student's *t* test for normally distributed data or a two-sided nonparametric Mann-Whitney *U* test for non-normally distributed data. $P < 0.05$ was defined as statistically significant. $^*P < 0.05$, $^{**}P < 0.01$, and $^{***}P < 0.001$.

Supplementary Materials

This PDF file includes:
Figs. S1 to S6
Legend for table S1

Other Supplementary Material for this manuscript includes the following:
Table S1

REFERENCES AND NOTES

1. M. Florio, W. B. Huttner, Neural progenitors, neurogenesis and the evolution of the neocortex. *Development* **141**, 2182–2194 (2014).
2. A. Kriegstein, A. Alvarez-Buylla, The glial nature of embryonic and adult neural stem cells. *Annu. Rev. Neurosci.* **32**, 149–184 (2009).
3. D. H. Rowitch, A. R. Kriegstein, Developmental genetics of vertebrate glial-cell specification. *Nature* **468**, 214–222 (2010).
4. E. Nutma, D. van Gent, S. Amor, L. A. N. Peferoen, Astrocyte and oligodendrocyte cross-talk in the central nervous system. *Cell* **9**, (2020).
5. C. Liu, J. C. Sage, M. R. Miller, R. G. Verhaak, S. Hippenmeyer, H. Vogel, O. Foreman, R. T. Bronson, A. Nishiyama, L. Luo, H. Zong, Mosaic analysis with double markers reveals tumor cell of origin in glioma. *Cell* **146**, 209–221 (2011).
6. K. Nakashima, M. Yanagisawa, H. Arakawa, N. Kimura, T. Hisatsune, M. Kawabata, K. Miyazono, T. Taga, Synergistic signaling in fetal brain by STAT3-Smad1 complex bridged by p300. *Science* **284**, 479–482 (1999).
7. L. Zhang, X. He, L. Liu, M. Jiang, C. Zhao, H. Wang, D. He, T. Zheng, X. Zhou, A. Hassan, Z. Ma, M. Xin, Z. Sun, M. A. Lazar, S. A. Goldman, E. N. Olson, Q. R. Lu, Hdac3 Interaction with p300 histone acetyltransferase regulates the oligodendrocyte and astrocyte lineage fate switch. *Dev. Cell* **36**, 316–330 (2016).
8. M. Namihira, J. Kohyama, K. Semi, T. Sanosaka, B. Deneen, T. Taga, K. Nakashima, Committed neuronal precursors confer astrocytic potential on residual neural precursor cells. *Dev. Cell* **16**, 245–255 (2009).
9. S. M. Glasgow, W. Zhu, C. C. Stolt, T. W. Huang, F. Chen, J. J. LoTurco, J. L. Neul, M. Wegner, C. Mohila, B. Deneen, Mutual antagonism between Sox10 and NFIA regulates diversification of glial lineages and glioma subtypes. *Nat. Neurosci.* **17**, 1322–1329 (2014).
10. M. K. Taylor, K. Yeager, S. J. Morrison, Physiological Notch signaling promotes gliogenesis in the developing peripheral and central nervous systems. *Development* **134**, 2435–2447 (2007).
11. C. Siebel, U. Lendahl, Notch signaling in development, tissue homeostasis, and disease. *Physiol. Rev.* **97**, 1235–1294 (2017).

12. C. Giachino, J. L. Boulay, R. Ivanek, A. Alvarado, C. Tostado, S. Lugert, J. Tchorz, M. Coban, L. Mariani, B. Bettler, J. Lathia, S. Frank, S. Pfister, M. Kool, V. Taylor, A tumor suppressor function for notch signaling in forebrain tumor subtypes. *Cancer Cell* **28**, 730–742 (2015).
13. N. Kessaris, M. Fogarty, P. Iannarelli, M. Grist, M. Wegner, W. D. Richardson, Competing waves of oligodendrocytes in the forebrain and postnatal elimination of an embryonic lineage. *Nat. Neurosci.* **9**, 173–179 (2006).
14. O. Basak, C. Giachino, E. Fiorini, H. R. Macdonald, V. Taylor, Neurogenic subventricular zone stem/progenitor cells are Notch1-dependent in their active but not quiescent state. *J. Neurosci.* **32**, 5654–5666 (2012).
15. J. C. Luna-Escalante, P. Formosa-Jordan, M. Ibanes, Redundancy and cooperation in Notch intercellular signaling. *Development* **145**, (2017).
16. X. Li, G. Liu, L. Yang, Z. Li, Z. Zhang, Z. Xu, Y. Cai, H. Du, Z. Su, Z. Wang, Y. Duan, H. Chen, Z. Shang, Y. You, Q. Zhang, M. He, B. Chen, Z. Yang, Decoding cortical glial cell development. *Neurosci. Bull.* **37**, 440–460 (2021).
17. C. C. Stolt, S. Rehberg, M. Ader, P. Lommes, D. Riethmacher, M. Schachner, U. Bartsch, M. Wegner, Terminal differentiation of myelin-forming oligodendrocytes depends on the transcription factor Sox10. *Genes Dev.* **16**, 165–170 (2002).
18. Z. Liu, X. Hu, J. Cai, B. Liu, X. Peng, M. Wegner, M. Qiu, Induction of oligodendrocyte differentiation by Olig2 and Sox10: Evidence for reciprocal interactions and dosage-dependent mechanisms. *Dev. Biol.* **302**, 683–693 (2007).
19. C. C. Stolt, P. Lommes, E. Sock, M. C. Chaboissier, A. Schedl, M. Wegner, The Sox9 transcription factor determines glial fate choice in the developing spinal cord. *Genes Dev.* **17**, 1677–1689 (2003).
20. W. Sun, A. Cornwell, J. Li, S. Peng, M. J. Osorio, N. Aalling, S. Wang, A. Benraiss, N. Lou, S. A. Goldman, M. Nedergaard, SOX9 is an astrocyte-specific nuclear marker in the adult brain outside the neurogenic regions. *J. Neurosci.* **37**, 4493–4507 (2017).
21. J. D. Cahoy, B. Emery, A. Kaushal, L. C. Foo, J. L. Zamanian, K. S. Christopherson, Y. Xing, J. L. Lubischer, P. A. Krieg, S. A. Krupenko, W. J. Thompson, B. A. Barres, A transcriptome database for astrocytes, neurons, and oligodendrocytes: A new resource for understanding brain development and function. *J. Neurosci.* **28**, 264–278 (2008).
22. H. Huang, W. He, T. Tang, M. Qiu, Immunological markers for central nervous system glia. *Neurosci. Bull.*, (2023).
23. T. Stuart, A. Butler, P. Hoffman, C. Hafemeister, E. Papalexi, W. M. Mauck 3rd, Y. Hao, M. Stoeckius, P. Smibert, R. Satija, Comprehensive integration of single-cell data. *Cell* **177**, 1888–1902.e21 (2019).
24. J. P. Magnusson, C. Goritz, J. Tatarishvili, D. O. Dias, E. M. Smith, O. Lindvall, Z. Kokaia, J. Frisen, A latent neurogenic program in astrocytes regulated by Notch signaling in the mouse. *Science* **346**, 237–241 (2014).
25. D. S. Castro, B. Martynoga, C. Parras, V. Ramesh, E. Pacary, C. Johnston, D. Drechsel, M. Lebel-Potter, L. G. Garcia, C. Hunt, D. Dolle, A. Bithell, L. Ettwiller, N. Buckley, F. Guillemot, A novel function of the proneural factor Ascl1 in progenitor proliferation identified by genome-wide characterization of its targets. *Genes Dev.* **25**, 930–945 (2011).
26. I. Imayoshi, R. Kageyama, bHLH factors in self-renewal, multipotency, and fate choice of neural progenitor cells. *Neuron* **82**, 9–23 (2014).
27. H. Jiang, W. Bian, Y. Sui, H. Li, H. Zhao, W. Wang, X. Li, FBXO42 facilitates Notch signaling activation and global chromatin relaxation by promoting K63-linked polyubiquitination of RBPJ. *Sci. Adv.* **8**, eabq4831 (2022).
28. H. Ohnuki, H. Inoue, N. Takemori, H. Nakayama, T. Sakaue, S. Fukuda, D. Miwa, E. Nishiwaki, M. Hatano, T. Tokuhisa, Y. Endo, M. Nose, S. Higashiyama, BAZF, a novel component of cullin3-based E3 ligase complex, mediates VEGFR and Notch cross-signaling in angiogenesis. *Blood* **119**, 2688–2698 (2012).
29. X. Ge, G. Xiao, H. Huang, J. Du, Y. Tao, A. Yang, H. Wu, Z. Zhang, M. Qiu, Stage-dependent regulation of oligodendrocyte development and enhancement of myelin repair by dominant negative Master-mind 1 protein. *Glia* **67**, 1654–1666 (2019).
30. F. Siddiqi, F. Chen, A. W. Aron, C. G. Fiondella, K. Patel, J. J. LoTurco, Fate mapping by piggyBac transposase reveals that neocortical GLAST+ progenitors generate more astrocytes than Nestin+ progenitors in rat neocortex. *Cereb. Cortex* **24**, 508–520 (2014).
31. E. R. Andersson, R. Sandberg, U. Lendahl, Notch signaling: Simplicity in design, versatility in function. *Development* **138**, 3593–3612 (2011).
32. O. Ehm, C. Goritz, M. Covic, I. Schaffner, T. J. Schwarz, E. Karaca, B. Kempkes, E. Kremmer, F. W. Pfrieger, L. Espinosa, A. Bigas, C. Giachino, V. Taylor, J. Frisen, D. C. Lie, RBPJκ-dependent signaling is essential for long-term maintenance of neural stem cells in the adult hippocampus. *J. Neurosci.* **30**, 13794–13807 (2010).
33. A. Alzu'bi, G. J. Clowry, Expression of ventral telencephalon transcription factors ASCL1 and DLX2 in the early fetal human cerebral cortex. *J. Anat.* **235**, 555–568 (2019).
34. J. Du, M. Yi, F. Zhou, W. He, A. Yang, M. Qiu, H. Huang, S100B is selectively expressed by gray matter protoplasmic astrocytes and myelinating oligodendrocytes in the developing CNS. *Mol. Brain* **14**, 154 (2021).
35. T. Y. Vue, R. K. Kollipara, M. D. Borromeo, T. Smith, T. Mashimo, D. K. Burns, R. M. Bachoo, J. E. Johnson, ASCL1 regulates neurodevelopmental transcription factors and cell cycle genes in brain tumors of glioma mouse models. *Glia* **68**, 2613–2630 (2020).
36. J. Hou, H. Bi, Z. Ye, W. Huang, G. Zou, X. Zou, Y. S. Shi, Y. Shen, Q. Ma, F. Kirchhoff, Y. Hu, G. Chen, Pen-2 negatively regulates the differentiation of oligodendrocyte precursor cells into astrocytes in the central nervous system. *J. Neurosci.* **41**, 4976–4990 (2021).
37. M. A. Bonaguidi, T. McGuire, M. Hu, L. Kan, J. Samanta, J. A. Kessler, LIF and BMP signaling generate separate and discrete types of GFAP-expressing cells. *Development* **132**, 5503–5514 (2005).
38. M. T. Uemura, M. Ihara, T. Maki, T. Nakagomi, S. Kaji, K. Uemura, T. Matsuyama, R. N. Kalaria, A. Kinoshita, R. Takahashi, Pericyte-derived bone morphogenetic protein 4 underlies white matter damage after chronic hypoperfusion. *Brain Pathol.* **28**, 521–535 (2018).
39. I. A. Ciechomska, B. Gielniewski, B. Wojtas, B. Kaminska, J. Mieczkowski, EGFR/FOXO3a/BIM signaling pathway determines chemosensitivity of BMP4-differentiated glioma stem cells to temozolomide. *Exp. Mol. Med.* **52**, 1326–1340 (2020).
40. A. Saunders, E. Z. Macosko, A. Wysoker, M. Goldman, F. M. Krienen, H. de Rivera, E. Bien, M. Baum, L. Bortolin, S. Wang, A. Goeva, J. Nemesh, N. Kamitaki, S. Brumbaugh, D. Kulp, S. A. McCarroll, Molecular diversity and specializations among the cells of the adult mouse brain. *Cell* **174**, 1015–1030.e16 (2018).
41. T. Friedrich, F. Ferrante, L. Pioger, A. Nist, T. Stiewe, J. C. Andrau, M. Bartkuhn, B. D. Giaimo, T. Borggrefe, Notch-dependent and -independent functions of transcription factor RBPJ. *Nucleic Acids Res.* **50**, 7925–7937 (2022).
42. N. Camargo, A. Goudriaan, A. F. van Deijk, W. M. Otte, J. F. Brouwers, H. Lodder, D. H. Gutmann, K. A. Nave, R. M. Dijkhuizen, H. D. Mansvelder, R. Chrast, A. B. Smit, M. H. G. Verheijen, Oligodendroglial myelination requires astrocyte-derived lipids. *PLOS Biol.* **15**, e1002605 (2017).
43. W. Liedtke, W. Edelmann, P. L. Bieri, F. C. Chiu, N. J. Cowan, R. Kucherlapati, C. S. Raine, GFAP is necessary for the integrity of CNS white matter architecture and long-term maintenance of myelination. *Neuron* **17**, 607–615 (1996).
44. Z. An, O. Aksoy, T. Zheng, Q. W. Fan, W. A. Weiss, Epidermal growth factor receptor and EGFRvIII in glioblastoma: Signaling pathways and targeted therapies. *Oncogene* **37**, 1561–1575 (2018).
45. H. Zhu, J. Acquaviva, P. Ramachandran, A. Boskovitz, S. Woolfenden, R. Pfannl, R. T. Bronson, J. W. Chen, R. Weissleder, D. E. Housman, A. Charest, Oncogenic EGFR signaling cooperates with loss of tumor suppressor gene functions in gliomagenesis. *Proc. Natl. Acad. Sci. U.S.A.* **106**, 2712–2716 (2009).
46. S. I. Bannykh, C. C. Stolt, J. Kim, A. Perry, M. Wegner, Oligodendroglial-specific transcriptional factor SOX10 is ubiquitously expressed in human gliomas. *J. Neurooncol* **76**, 115–127 (2006).
47. F. Lu, Y. Chen, C. Zhao, H. Wang, D. He, L. Xu, J. Wang, X. He, Y. Deng, E. E. Lu, X. Liu, R. Verma, H. Bu, R. Drissi, M. Fouladi, A. O. Stemmer-Rachamimov, D. Burns, M. Xin, J. B. Rubin, E. M. Bahassi, P. Canoll, E. C. Holland, Q. R. Lu, Olig2-dependent reciprocal shift in PDGF and EGF receptor signaling regulates tumor phenotype and mitotic growth in malignant glioma. *Cancer Cell* **29**, 669–683 (2016).
48. Q. Weng, J. Wang, J. Wang, D. He, Z. Cheng, F. Zhang, R. Verma, L. Xu, X. Dong, Y. Liao, X. He, A. Potter, L. Zhang, C. Zhao, M. Xin, Q. Zhou, B. J. Aronow, P. J. Blackshear, J. N. Rich, Q. He, W. Zhou, M. L. Suva, R. R. Waclaw, S. S. Potter, G. Yu, Q. R. Lu, Single-cell transcriptomics uncovers glial progenitor diversity and cell fate determinants during development and gliomagenesis. *Cell Stem Cell* **24**, 707–723.e8 (2019).
49. R. G. Verhaak, K. A. Hoadley, E. Purdom, V. Wang, Y. Qi, M. D. Wilkerson, C. R. Miller, L. Ding, T. Golub, J. P. Mesirov, G. Alexe, M. Lawrence, M. O'Kelly, P. Tamayo, B. A. Weir, S. Gabriel, W. Winckler, S. Gupta, L. Jakkula, H. S. Feiler, J. G. Hodgson, C. D. James, J. N. Sarkaria, C. Brennan, A. Kahn, P. T. Spellman, R. K. Wilson, T. P. Speed, J. W. Gray, M. Meyerson, G. Getz, C. M. Perou, D. N. Hayes, Cancer Genome Atlas Research Network, Integrated genomic analysis identifies clinically relevant subtypes of glioblastoma characterized by abnormalities in PDGFRA, IDH1, EGFR, and NF1. *Cancer Cell* **17**, 98–110 (2010).
50. T. Y. Vue, E. J. Kim, C. M. Parras, F. Guillemot, J. E. Johnson, Ascl1 controls the number and distribution of astrocytes and oligodendrocytes in the gray matter and white matter of the spinal cord. *Development* **141**, 3721–3731 (2014).
51. D. P. Kelenis, E. Hart, M. Edwards-Fligner, J. E. Johnson, T. Y. Vue, ASCL1 regulates proliferation of NG2-glia in the embryonic and adult spinal cord. *Glia* **66**, 1862–1880 (2018).
52. M. Zamboni, E. Llorens-Bobadilla, J. P. Magnusson, J. Frisen, A widespread neurogenic potential of neocortical astrocytes is induced by injury. *Cell Stem Cell* **27**, 605–617. e5 (2020).
53. J. E. Herrmann, T. Imura, B. Song, J. Qi, Y. Ao, T. K. Nguyen, R. A. Korsak, K. Takeda, S. Akira, M. V. Sofroniew, STAT3 is a critical regulator of astrogliosis and scar formation after spinal cord injury. *J. Neurosci.* **28**, 7231–7243 (2008).
54. H. Kiray, S. L. Lindsay, S. Hosseinzadeh, S. C. Barnett, The multifaceted role of astrocytes in regulating myelination. *Exp. Neurol.* **283**, 541–549 (2016).

55. W. Huang, N. Zhao, X. Bai, K. Karram, J. Trotter, S. Goebbels, A. Scheller, F. Kirchhoff, Novel NG2-CreERT2 knock-in mice demonstrate heterogeneous differentiation potential of NG2 glia during development. *Glia* **62**, 896–913 (2014).
56. A. I. Son, S. Mohammad, T. Sasaki, S. Ishii, S. Yamashita, K. Hashimoto-Torii, M. Torii, Dual role of rbpj in the maintenance of neural progenitor cells and neuronal migration in cortical development. *Cereb. Cortex* **30**, 6444–6457 (2020).
57. M. Brenner, A. B. Johnson, O. Boespflug-Tanguy, D. Rodriguez, J. E. Goldman, A. Messing, Mutations in GFAP, encoding glial fibrillary acidic protein, are associated with Alexander disease. *Nat. Genet.* **27**, 117–120 (2001).
58. L. Li, E. Tian, X. Chen, J. Chao, J. Klein, Q. Qu, G. Sun, G. Sun, Y. Huang, C. D. Warden, P. Ye, L. Feng, X. Li, Q. Cui, A. Sultan, P. Douvaras, V. Fossati, N. E. Sanjana, A. D. Riggs, Y. Shi, GFAP Mutations in Astrocytes Impair Oligodendrocyte Progenitor Proliferation and Myelination in an hiPSC Model of Alexander Disease. *Cell Stem Cell* **23**, 239–251.e6 (2018).
59. S. Zhang, Y. Wang, X. Zhu, L. Song, X. Zhan, E. Ma, J. McDonough, H. Fu, F. Cambi, J. Grinspan, F. Guo, The Wnt Effector TCF7l2 promotes oligodendroglial differentiation by repressing autocrine BMP4-mediated signaling. *J. Neurosci.* **41**, 1650–1664 (2021).
60. R. D. McKinnon, S. Waldron, M. E. Kiel, PDGF α-Receptor signal strength controls an RTK rheostat that integrates phosphoinositol 3′-kinase and phospholipase Cγ pathways during oligodendrocyte maturation. *J. Neurosci.* **25**, 3499–3508 (2005).
61. B. Stankoff, M. S. Aigrot, F. Noel, A. Wattilliaux, B. Zalc, C. Lubetzki, Ciliary neurotrophic factor (CNTF) enhances myelin formation: A novel role for CNTF and CNTF-related molecules. *J. Neurosci.* **22**, 9221–9227 (2002).
62. N. Miyamoto, T. Maki, A. Shindo, A. C. Liang, M. Maeda, N. Egawa, K. Itoh, E. K. Lo, J. Lok, M. Ihara, K. Arai, Astrocytes promote oligodendrogenesis after white matter damage via brain-derived neurotrophic factor. *J. Neurosci.* **35**, 14002–14008 (2015).
63. Q. Weng, Y. Chen, H. Wang, X. Xu, B. Yang, Q. He, W. Shou, Y. Chen, Y. Higashi, V. van den Berghe, E. Seuntjens, S. G. Kernie, P. Bukshpun, E. H. Sherr, D. Huylebroeck, Q. R. Lu, Dual-mode modulation of Smad signaling by Smad-interacting protein Sip1 is required for myelination in the central nervous system. *Neuron* **73**, 713–728 (2012).
64. J. See, P. Mamontov, K. Ahn, L. Wine-Lee, E. B. Crenshaw 3rd, J. B. Grinspan, BMP signaling mutant mice exhibit glial cell maturation defects. *Mol. Cell. Neurosci.* **35**, 171–182 (2007).
65. J. P. Magnusson, M. Zamboni, G. Santopolo, J. E. Mold, M. Barrientos-Somarribas, C. Talavera-Lopez, B. Andersson, J. Frisen, Activation of a neural stem cell transcriptional program in parenchymal astrocytes. *eLife* **9**, (2020).
66. S. Y. Kong, W. Kim, H. R. Lee, H. J. Kim, The histone demethylase KDM5A is required for the repression of astrocytogenesis and regulated by the translational machinery in neural progenitor cells. *FASEB J.* **32**, 1108–1119 (2018).
67. H. Tabata, Diverse subtypes of astrocytes and their development during corticogenesis. *Front. Neurosci.* **9**, 114 (2015).
68. O. A. Bayraktar, T. Bartels, S. Holmqvist, V. Kleshchevnikov, A. Martirosyan, D. Polioudakis, L. Ben Haim, A. M. H. Young, M. Y. Batiuk, K. Prakash, A. Brown, K. Roberts, M. F. Paredes, R. Kawaguchi, J. H. Stockley, K. Sabeur, S. M. Chang, E. Huang, P. Hutchinson, E. M. Ullian, M. Hemberg, G. Coppola, M. G. Holt, D. H. Geschwind, D. H. Rowitch, Astrocyte layers in the mammalian cerebral cortex revealed by a single-cell in situ transcriptomic map. *Nat. Neurosci.* **23**, 500–509 (2020).
69. J. Chen, Y. Li, T. S. Yu, R. M. McKay, D. K. Burns, S. G. Kernie, L. F. Parada, A restricted cell population propagates glioblastoma growth after chemotherapy. *Nature* **488**, 522–526 (2012).
70. S. K. Singh, C. Hawkins, I. D. Clarke, J. A. Squire, J. Bayani, T. Hide, R. M. Henkelman, M. D. Cusimano, P. B. Dirks, Identification of human brain tumour initiating cells. *Nature* **432**, 396–401 (2004).
71. H.-K. Liu, Y. Wang, T. Belz, D. Bock, A. Takacs, B. Radlwimmer, S. Barbus, G. Reifenberger, P. Lichter, G. Schütz, The nuclear receptor tailless induces long-term neural stem cell expansion and brain tumor initiation. *Genes Dev.* **24**, 683–695 (2010).
72. L. Zhuo, M. Theis, I. Alvarez-Maya, M. Brenner, K. Willecke, A. Messing, hGFAP-cre transgenic mice for manipulation of glial and neuronal function in vivo. *Genesis* **31**, 85–94 (2001).
73. H. Han, K. Tanigaki, N. Yamamoto, K. Kuroda, M. Yoshimoto, T. Nakahata, K. Ikuta, T. Honjo, Inducible gene knockout of transcription factor recombination signal binding protein-J reveals its essential role in T versus B lineage decision. *Int. Immunol.* **14**, 637–645 (2002).
74. U. Schüller, V. M. Heine, J. Mao, A. T. Kho, A. K. Dillon, Y.-G. Han, E. Huillard, T. Sun, A. H. Ligon, Y. Qian, Q. Ma, A. Alvarez-Buylla, A. P. McMahon, D. H. Rowitch, K. L. Ligon, Acquisition of granule neuron precursor identity is a critical determinant of progenitor cell competence to form Shh-induced medulloblastoma. *Cancer Cell* **14**, 123–134 (2008).
75. Q. Xu, M. Tam, S. A. Anderson, Fate mapping Nkx2.1-lineage cells in the mouse telencephalon. *J. Comp. Neurol.* **506**, 16–29 (2008).
76. M. He, J. Tucciarone, S. Lee, M. J. Nigro, Y. Kim, J. M. Levine, S. M. Kelly, I. Krugikov, P. Wu, Y. Chen, L. Gong, Y. Hou, P. Osten, B. Rudy, Z. J. Huang, Strategies and tools for combinatorial targeting of GABAergic neurons in mouse cerebral cortex. *Neuron* **91**, 1228–1243 (2016).
77. X. Song, H. Chen, Z. Shang, H. Du, Z. Li, Y. Wen, G. Liu, D. Qi, Y. You, Z. Yang, Z. Zhang, Z. Xu, Homeobox Gene *Six3* is required for the differentiation of D2-Type medium spiny neurons. *Neurosci. Bull.* **37**, 985–998 (2021).
78. Z. Xu, Q. Liang, X. Song, Z. Zhang, S. Lindtner, Z. Li, Y. Wen, G. Liu, T. Guo, D. Qi, M. Wang, C. Wang, H. Li, Y. You, X. Wang, B. Chen, H. Feng, J. L. Rubenstein, Z. Yang, SP8 and SP9 coordinately promote D2-type medium spiny neuron production by activating *Six3* expression. *Development* **145**, dev165456 (2018).

Acknowledgments: We are grateful to H. Han for providing the *Rbpj* floxed mice. **Funding:** This work was supported by grants from the National Key Research and Development Program of China (2018YFA0108000), the National Natural Science Foundation of China (32200792, 31630032, 31820103006, 32100768, and 32070971), a Shanghai Municipal Science and Technology Major Project (2018SHZDZX01), ZJLab, grants from NIH (R01MH094589 and R01NS089777), and a Natural Science Foundation of Shanghai (20ZR1452500). **Author contributions:** Z.X., X.L., and Z.Y. conceptualized the project, and Z.Y. supervised the project. Z. X. and R.G. analyzed the data. R.G., D.H., X.S., and Y.G. performed most of the experiments. Z.L. performed the cell sorting. Z.X. designed the experiments, produced all figures, and wrote the manuscript with input from all authors. **Competing interests:** The authors declare that they have no competing interests. **Data and materials availability:** All data needed to evaluate the conclusions in the paper are present in the paper and/or the Supplementary Materials. Raw and processed sequencing data generated in this study have been deposited on NCBI GEO under the accession code GSE240224. P35 tumor and adult frontal mouse cortex scRNA-seq data were obtained from GEO (GSE122871 and GSE116470). The *Rbpj* floxed mice can be provided by H. Han pending scientific review and a completed material transfer agreement. Requests for the *Rbpj* floxed mice should be submitted to huahan@fmmu.edu.cn.

Submitted 11 April 2023
Accepted 11 October 2023
Published 10 November 2023
10.1126/sciadv.adi2167

ScienceAdvances

Context-dependent regulation of Notch signaling in glial development and tumorigenesis

Rongliang Guo, Danyu Han, Xingrui Song, Yanjing Gao, Zhenmeiyu Li, Xiaosu Li, Zhengang Yang, and Zhejun Xu

Sci. Adv. **9** (45), eadi2167. DOI: 10.1126/sciadv.adi2167